Final Technical Report: 01HQGR0025
Ground-motion Relations for Puerto Rico

Dariush Motazedian & Gail Atkinson

Non-technical Summary

Ground-motion relations were developed for Puerto Rico, which describe the strength of shaking as a function of earthquake magnitude and distance. The work is based on ground-motion data recorded at Puerto Rican seismographic stations. The ground-motion relations from this research provide the foundation for seismic hazard maps and engineering analyses for Puerto Rico. The research products can be directly used by engineers working in seismic-resistant design and dynamic-response analyses of buildings.

Abstract

Fourier amplitudes and response spectra of more than 3000 waveforms from about 300 Puerto Rico earthquakes of magnitude 3 to 5.5 have been analyzed. Due to a paucity of data at small distances and large magnitudes, the ground-motion data cannot be used directly to obtain ground-motion relations for magnitudes and distances of most engineering interest. Instead the data were used to determine key attenuation parameters, such as regional Q, duration behavior and generic site amplification that are input to seismological ground-motion models. The data were also used to validate ground-motion model predictions.

To overcome the incompleteness of the data set we applied the stochastic method to simulate waveforms for different magnitudes and distances. The stochastic method has been applied for other regions such as California, Cascadia, and Eastern North America, and on average reproduces empirical attenuation relationships that can be obtained by direct use of enough data. The input parameters for the simulations are based on the attenuation parameters obtained from the recorded waveforms.

We simulated 1950 acceleration time series for magnitudes from **M**3.0 to **M**8.0 and distances from 2 km to 500 km. Simulation is performed in magnitude steps of 0.2 units. In order to provide a good database we simulated data for both backward and forward directivity cases, as well as data for azimuths with minimal directivity effects. The response spectra of the simulated time series have been calculated. The maximum likelihood method has been applied in order to derive ground-motion relations for a generic soft rock site condition (NEHRP C), for frequencies from 0.1 to 20Hz. The stochastic-model ground-motion relations for Puerto Rico are validated using available seismographic data, and compared to ground-motion relations for other regions. These are the first region-specific ground-motion relations developed for seismic hazard analysis of Puerto Rico.

Introduction

Puerto Rico has a high level of seismic activity due to its location on the boundary between the North American and the Caribbean plates. At least four destructive earthquakes are documented in the historical records before 1700. There was a possible great earthquake in 1787 (**M**8 to 8.2), and a major earthquake in 1918 (**M**7.3) (McCann, 1985, 2002a). About 9000 earthquakes of M>3 have been recorded since the inception of the Puerto Rico Seismic Network in 1974 (McCann, 2002a). A felt seismic event occurs about once per month. Thus Puerto Rico's 3.8 million inhabitants are exposed to a significant earthquake hazard.

Despite the hazard, there are to date no region-specific ground-motion relations for Puerto Rico. Ground-motion relations, describing the expected amplitudes of ground motions as functions of magnitude and distance, are a key component of seismic hazard analyses. In order to provide accurate seismic hazard assessments for Puerto Rico – a prerequisite for making informed seismic design decisions – it is important to develop such ground-motion relations. In this paper, we develop ground-motion relations for Puerto Rico, using a combination of seismological and empirical modeling. We use data recorded on regional broadband and local seismic networks to determine the underlying attenuation parameters and validate the predictions of the ground-motion relations. First, we describe the overall method that is employed to define ground-motion relations. Then, we describe the Puerto Rico ground-motion data and how they are used to obtain underlying attenuation parameters for the model. We then present the simulated ground-motion database and use it to derive ground-motion relations. Finally, we compare the derived relations to recorded data and to ground-motion relations for other regions.

Method

The stochastic model is a widely-used tool to simulate acceleration time series and develop ground-motion relations (Hanks and McGuire, 1981; Boore, 1983; Atkinson and Boore, 1995 and 1997; Toro et al., 1997; Atkinson and Silva, 2000). The stochastic method begins with the specification of the Fourier spectrum of ground motion as a function of magnitude and distance. Often the acceleration spectrum is modeled by a spectrum with an ω^2 shape, where ω= angular frequency (Aki, 1967; Brune, 1970, 1971; Boore 1983). The "Brune model" spectrum is derived for an instantaneous shear dislocation at a point. The acceleration spectrum of the shear wave, A(f), at hypocentral distance R from an earthquake is given by:

$$A(f) = CM_0 (2\pi f)^2 / [1+ f/ f_0)^2] \exp(-\pi f \kappa) \exp(-\pi f R/Q\beta)/R \qquad (1)$$

where M_0 is seismic moment and f_0 is corner frequency, which is given by f_0= $4.9*10^6 \beta (\Delta\sigma / M_0)^{1/3}$ where $\Delta\sigma$ is stress drop in bars, M_0 is in dyne-cm, and

β is shear wave velocity in km/s (Boore, 1983). The constant C= $\Re^{\theta\varphi}$ F V /($4\pi\rho\beta^3$), where $\Re^{\theta\varphi}$ = radiation pattern (average value of 0.55 for shear waves), F= free surface amplification (2.0), V= partition onto two horizontal components (0.71), ρ= density, and R= hypocentral distance (Boore, 1983). The term exp (-$\pi f\kappa$) is a high-cut filter to account for near-surface "*kappa*" effects, which describe the commonly observed rapid spectral decay at high frequencies (Anderson and Hough, 1984). In the above equation the power of R in the denominator of the attenuation term, exp (-πf R/Q β)/R, is considered equal to 1, which is appropriate for body-wave spreading in a whole space. This value can be changed as needed in order to account for the presence of postcritical reflections from the Moho discontinuity or multiply reflected waves traveling in the crustal waveguide. The quality factor, *Q*(*f*), is an inverse measure of anelastic attenuation . Through this equation, the spectrum is diminished with distance to account for empirically-defined attenuation behavior.

Finite fault modeling has been an important tool for the prediction of ground motion near the epicenters of large earthquakes (Hartzel, 1978; Irikura, 1983; Joyner and Boore, 1986; Heaton and Hartzel, 1986; Somerville et al., 1991; Tumarkin and Archuleta, 1994; Zeng et al., 1994; Beresnev and Atkinson, 1998a). One of the most useful methods to simulate ground motion for a large earthquake is based on the simulation of a number of small earthquakes as subfaults that comprise a big fault. A large fault is divided into N subfaults and each subfault is considered as a small point source (introduced by Hartzel, 1978). Ground motions of subfaults, each of which may be calculated by the stochastic point-source method as described above, are summed with a proper delay time in the time domain to obtain the ground motion from the entire fault, a (t):

$$a(t)= \sum_{i=1}^{nl} \sum_{j=1}^{nw} a_{ij}(t+\Delta t_{ij}) \qquad (2)$$

where *nl* and *nw* are the number of subfaults along the length and width of main fault, respectively (*nl**nw* = N), Δt_{ij} is the relative delay time for the radiated wave from the ij^{th} subfault to reach the observation point. The $a_{ij}(t)$ are each calculated by the stochastic point source method.

The stochastic method has also been used to derive ground-motion relations for many different regions. Atkinson and Boore (1995) derived ground-motion relations for eastern North America, using a stochastic point-source model with an empirical two-corner source model. Toro *et al.* (1997) developed similar relations for eastern North America using a Brune point-source model. Atkinson and Silva (2000) developed ground-motion relations for California using a stochastic method that exploits the equivalence between the finite fault model and a two-corner point-source model of the earthquake spectrum. In each of these cases, region-specific input parameters derived from seismograms were used to specify the model parameters that drive the ground-motion relations for that region. For

California, where there is a good empirical strong-motion database, it was shown that the stochastic relations agree well with empirical regression equations (e.g. Abrahamson and Silva, 1997; Boore et al, 1997; Sadigh et al., 1997; Atkinson and Silva, 2000). The stochastic ground-motion relations provide a sound basis for estimating peak ground motions and response spectra for earthquakes of magnitude 4 through 8, at distances from 1 to 200 km over the frequency range 0.2 to 20 Hz.

In this study, we use a stochastic finite-fault approach. A modified version of the computer program FINSIM (Beresnev and Atkinson, 1998b) was used for the simulations. The modifications to FINSIM introduce the new concept of a "dynamic corner frequency" to more closely model real finite-fault dynamic behavior (appendix A). The modified program has been renamed EXSIM (Extended earthquake fault simulation program). EXSIM model parameters that represent the earthquake source processes have been calibrated for general applications, using data from 27 moderate to large well-recorded earthquakes in California. For use in Puerto Rico, the model requires region-specific attenuation and generic site parameters, which are derived from recordings of small-to-moderate earthquakes.

EXSIM is used to simulate a ground-motion database from which to develop ground-motion equations. We take this approach because there are not enough real data in the magnitude-distance ranges of engineering interest. We can use the empirical data to establish the underlying parameters and validate the model predictions. The region-specific parameters needed for simulations are:

1. Attenuation of Fourier amplitudes with distance (geometric spreading and Q-value);
2. Duration of ground motion as a function of magnitude and distance; and
3. Regional generic crust/site amplification.

With these parameters established, we can use the calibrated EXSIM model to extend our prediction to the magnitude-distance range of interest. We then compare predictions with Puerto Rico data and with ground-motion relations for other regions.

Ground-motion data for Puerto Rico

The Puerto Rico Seismic Network (PRSN), consisting of 13 vertical component short-period 1Hz natural frequency seismometers, was installed in 1974. Digital time series have been recorded by the PRSN since 1991 in IASPEI (International Association of Seismology and Physics of the Earth's Interior) format (16-bit Analogue to digital converter converter, 100 samples/Sec). More than 2000 time series recorded by the PRSN, from more than 300 events with $M \geq 3.0$ have been compiled; however many records were clipped and could not be used (Note: M refers to catalog magnitude, to be discussed in a later section). Time series recorded before 1991 cannot be used due to lack of information about

the instrument responses. Nine new three component broadband stations are being installed as of 2000 and will soon provide additional data.

The Puerto Rico Strong Motion Network (PRSMN) has been installed gradually since 1994, and now comprises 32 strong motion stations. The number of recorded acceleration time series is limited, since the earthquake ground motion must be strong enough to trigger these accelerographs. About 30 acceleration time series from 4 events are available from this network.

There has been a single IRIS (The Incorporated Research Institutions for Seismology)/USGS station (SJG) operating in Puerto Rico since 1993; it includes five broadband seismometers (three-component), and one short period seismometer (three-component). The sampling rate of the short period three-component seismometers is 80 samples/sec. The highest sampling rate for the broadband seismometer data is 20 samples/sec. From the SJG station, 1289 time series from more than 300 events with $M \geq 3.0$ have been compiled. These are the data with highest reliability, and well-known instrument response.

In order to study ground-motion processes, we need to remove all instrument response effects from the records, so that we can obtain the actual motion of the ground. Instrument-corrected data allow compilation of a regional ground-motion database in a uniform format for ground-motion studies. The instrument response of all stations was obtained from a detailed calibration program that included in-situ field calibrations of instruments using a portable seismograph with well-known response, and by calibration against the well-known response of the SJG station. The stability over time of the obtained instrument responses of the PRSN stations was also examined by plotting the residuals (e.g. deviations from calculated model values) of the Fourier spectra versus time for all of the recorded data. Data for which the instrument response could not be reliably determined were deleted from the database.

Fourier amplitudes and response spectra of more than 3000 time series (of known/calibrated instrument response) from more than 300 earthquakes in the Puerto Rico region were analyzed. Figure 1 shows the distribution of the ground-motion database by magnitude and distance. The databases can be obtained by sending a request to the first author (dariush@ccs.carleton.ca). Table 1 lists the moment magnitude for each event. The determination of these magnitudes is discussed later.

The shear-wave portion of signal and pre-event noise were windowed for all of the time series. We compiled data for which the signal to noise ratio was at least a factor of 2. For each record, the time series were processed as follows:

- Define S-window (shear wave window) and pre-event noise (minimum 10-second noise window was used for calculation of signal to noise ratio).
- Remove any glitches.
- Taper the windowed time series using a 5% taper on each end of the signal.

- Zero-Pad the time series to the next greatest power of 2.
- Transfer to frequency domain by Fast Fourier Transform.
- Calculate instrument response based on the poles, zeros and constant for that specified component of the seismographic station.
- Remove the instrument response in the frequency domain by dividing the recorded spectrum by the complex instrument transfer function.
- Convert Fourier spectra of velocity to Fourier spectra of acceleration (done in the frequency domain in the same step as removal of instrument response).
- Transfer to time domain by applying the inverse Fourier transform.
- Calculate response spectra for 5% damping from corrected acceleration time series.
- Discard the frequencies with signal to noise ratio less than 2 (Note: the noise window is normalized to the same length as the signal window to check the signal/noise ratio.)
- Smooth the Fourier spectra by using a weighted 9-point smoothing algorithm.

Determination of regional attenuation parameters

The key to the stochastic simulation model is the specification of the Fourier acceleration spectrum as a function of magnitude and distance. In order to specify the Fourier spectrum, we need the parameters that prescribe the earthquake source level, attenuation of ground motion and site response. Previous studies have determined that the overall source parameters for stochastic finite fault modeling are generic, and do not vary significantly by region (Atkinson and Boore, 1998; Beresnev and Atkinson, 2001). Thus the basic model is already well established by the calibration of EXSIM to the California strong motion database. The necessary regional attenuation parameters are the geometric spreading and the coefficient of anelastic attenuation. Other region-specific parameters describe amplification through the crustal velocity profile, including any regional generic soil responses. We also need to know the duration of shaking.

In this section we determine the duration of seismic waves and the geometric and anelastic attenuation parameters, all based on the recorded ground-motion data in Puerto Rico. This sets the stage for stochastic simulations to provide regional ground-motion relations satisfying the immediate and most significant needs of the engineering community for seismic design applications.

Ground-motion attenuation model

The frequency-dependent attenuation of Fourier amplitudes can be determined from ground-motion data by regression analysis, as described by

Atkinson and Mereu (1992). These regressions may also be used to determine source amplitudes for specific events, and relative site terms for all stations.

Fourier amplitudes can be fit to an equation of the form:

$$\log A_{ij}(f, R) = \log A_{i0}(f) - b \log R_{ij} - c(f) R_{ij} + \log S_j(f) \qquad (3)$$

where $A_{ij}(f)$ is the observed spectral amplitude of earthquake i at station j, for frequency f; $A_{i0}(f)$ is the source amplitude of earthquake i, R is hypocentral distance, b is the geometric spreading coefficient, $c(f)$ is the coefficient of anelastic attenuation, and $S_j(f)$ is the site response term for station j (Shin and Herrmann, 1987; Atkinson and Mereu, 1992). The anelastic coefficient, $c(f)$, is inversely related to the quality factor, Q:

$$Q = [\log(e)\, \pi f]/(c\, \beta), \qquad (4)$$

where β is the shear-wave velocity and e= 2.718 . Equation (3) may be applied to any ground-motion phase; the shear-wave phases are of most engineering interest, since they have the largest amplitudes (typically about five times larger than the *P*-wave amplitudes).

In developing the attenuation model, we must determine whether the ground-motion database can be adequately fit with a single geometric spreading rate b, or whether this coefficient will take on different values depending on the epicentral distance range. For example, in eastern North America, the attenuation is described by a "hinged-trilinear" form (Atkinson and Boore, 1995) in which geometric attenuation goes as R^{-1} to 70 km, then as R^0 for 70 to 130 km, then $R^{-1/2}$ beyond 130 km. This behavior is explained by the presence of strong post-critical reflections from the Moho discontinuity that cause "flattening" of the attenuation curve, leading to almost no apparent geometric spreading between approximately 70 and 130 km. It follows that the details of the empirical attenuation provide valuable clues as to the regional crustal structure and the presence of major velocity discontinuities that affect ground-motion amplitudes.

In order to find the hinge points of the attenuation curve, representing the transition from direct S-wave to post-critical Moho reflection, we applied a trial profile of different hinge points to equation 3 using the ground-motion database to determine the best-fit model. The first hinge point is incremented from 40 to 105 km by 5 km steps. The second hinge, representing the transition to surface–wave spreading, is incremented from 40 to 150 km with the same step distance. For each pair of hinge points, the maximum likelihood method (Joyner and Boore, 1993) has been applied to equation 3, to determine the value of the coefficients. Then the residuals for all records, for frequencies from 0.1 to 8 Hz, have been calculated. (Note: residual= (log of observed A_{ij}) – (log of predicted A_{ij}) by equation 3). Hinge points at 75 and 100 km produce the lowest averaged

residuals. As Figure 2 shows, with hinge points at 75 and 100 km the regression residuals have a good distribution versus distance, with no trend. Thus we adopt a geometric spreading model of R^{-1}, R^{0}, $R^{-0.5}$ for the simulations, with hinge points at 75 and 100 km.

Q-Value

Equation 3 has been solved by the maximum likelihood method (Joyner and Boore, 1993) to obtain the geometric spreading coefficient *b*, and the frequency-dependent attenuation *c*, providing a description of regional path effects. In this section we are principally interested in the frequency-dependent attenuation coefficient *c,* which is related to the regional Q-value through equation 4. Figure 3 shows the determined Q values for shallow ($h \leq 30$ km) and deep ($h > 30$ km) earthquakes in Puerto Rico. The standard error of the mean Q-values spans a wider range than the difference between Q-values for the deep and shallow earthquake subsets. Thus we can fit both deep and shallow earthquakes using a single Q model: when the data are combined, the Q-values are described by the equation:

$$Q = 359\, f^{0.59} \qquad (5)$$

as shown in Figure 3. Figure 3 also compares the Q values obtained for Puerto Rico to Q-values for Eastern North America (Atkinson and Boore, 1995) and California (Raoof et al., 1999). The Puerto Rico Q-values are intermediate to those for ENA (Eastern North America) and California.

Duration of ground motion

The duration (T) of an earthquake signal at hypocentral distance *R* can generally be represented as (Atkinson and Boore, 1995):

$$T(R) = T_0 + dR,$$

where T_0 is the source duration, and *d* is the coefficient controlling the increase of duration with distance; *d* is derived empirically. *d* may be a single coefficient describing all distances of interest (eg. Atkinson, 1995), or it can take different values depending on the distance range (eg. Atkinson and Boore, 1995).

Using the Puerto Rico ground-motion data, we developed an empirical model of the distance-dependence of duration. For each record the measured duration, including the strong part of the shaking, was assumed to be represented

by $T(R)=T_0+dR$. The source duration (T_0) is short (< 1 sec) for these records due to their small magnitudes and can thus be neglected. Figure 4 compares the duration behavior with distance for Puerto Rico with that of Eastern North America (using ENA data of Atkinson and Boore 1995, which are defined using an rms duration definition consistent with the stochastic model). In this figure the Y-axis is $T(R)$ - T_0 where the source duration is estimated as T_0 = 1/2 f_A, with $\log(f_A)$= 2.41 - 0.533**M** (Atkinson and Boore, 1995). The change of slope at around 75 and 100 km again suggests a trilinear attenuation curve for the Puerto Rico region, similar to observations for Eastern North America (Atkinson and Boore, 1995). The larger amount of scatter in the Puerto Rico data in Figure 4, compared to ENA data, is due to several factors. The first factor could be the greater variability of site conditions in Puerto Rico. Soil sites cause more scattered duration data than rock sites. Differences in the wave propagation behavior in the complex tectonic regime of Puerto Rico, especially for deeper events could be another reason for the large amount of scatter. In addition in Puerto Rico there is a mixture of different types of seismic sources, including in-slab, interface and crustal earthquakes. Finally, the durations for Puerto Rico were measured subjectively from the records, while those for ENA were calculated from an analytical duration definition. Based on Figure 4 we adopt the ENA duration model of Atkinson and Boore (1995) with the obtained hinge points for Puerto Rico (75 and 100 km) for the simulations.

H/V ratio (generic regional amplification effects)

The ratio of the horizontal to vertical component of ground motion (H/V) is an important parameter since most of the seismographic stations in Puerto Rico record only the vertical component, whereas the horizontal component is of primary engineering interest. The H/V ratio is believed to reflect amplification effects, both from the crustal velocity gradient, and from near-surface soils (Nakamura 1989, Atkinson and Cassidy, 2000; Lermo and Chavez-Garcia, 1993). Earthquake waves propagate from the source region, where the shear wave velocity is typically about 3.6 km/sec, towards the surface, where the average shear wave velocity may be around 620 m/sec for generic soft rock sites (Boore and Joyner, 1997). The spectrum will be amplified through this velocity gradient by seismic impedance effects. Amplification effects are observed strongly on the horizontal component, but only weakly on the vertical component (due to the turning of rays towards the vertical by refraction). Hence the H/V ratio is a rough measure of site amplification.

Most of the PRSN data collected to date are vertical-component recordings. However, there are also a limited number of three-component data available. We used the three-component data to establish an empirical relationship between horizontal and vertical component amplitudes. This makes it possible to use the entire PRSN database in the development of regional ground-motion relations.

Figure 5 compares H/V ratios for the IRIS 3-component broadband station in Puerto Rico (SJG) with the observed H/V ratios for various NEHRP (U.S.

National Earthquake Hazards Reduction Program) site classes in other regions. The NEHRP site classes describe the soil conditions by the average shear-wave velocity (v_s) over the top 30m. (NEHRP A= ($v_{s.}$>1500 m/s), B= (760-1,500 m/s), C= (360-760 m/s), D= (180-360 m/s) and E= (< 180 m/s), Borcherdt, 1995). Information on H/V ratio for these other regions is given in Chen (2000) and Chen and Atkinson (2002). We make the assumption that the observed H/V ratio is an estimate of the amplification of the horizontal component due to regional site effects. The observed H/V at SJG suggests an amplification at high frequencies, which probably means that there is a thin soft layer under the site (e.g. the frequency of amplification is inversely proportional to the thickness of the amplifying layer, while the degree of amplification depends on the seismic impedance contrast). The trend of H/V at the SJG station in Puerto Rico looks very much like the trend of the H/V ratios for shallow soil sites in Japan that may be classified as NEHRP B or C. For the 45 stations in the Japan data set that are so classified (by Chen, 2000) the average shear wave velocity over the top 30 m is about 738 m/sec (NEHRP C), and the average layer thickness (over rock) is about 11 m (Chen and Atkinson, 2002).

For simulation of ground motions in Puerto Rico the obtained H/V at SJG will be applied as a generic site amplification for all sites. Based on the observations made at sites, all appear to be similar in terms of site conditions. They can be characterized as soft rock sites, and likely have a weathered layer that overlies harder rock. They are probably NEHRP B or NEHRP C in terms of shear-wave velocity. (Note: an improvement on this assumption will be possible in future applications, as studies being conducted by J. Martinzez-Cruzado at the University of Puerto Rico, Mayaguez, are establishing the shear-wave velocity profiles of sites across Puerto Rico.)

Simulation of acceleration time series

Acceleration time series for earthquakes with magnitudes from **M**3.0 to **M**8.0 (where **M** is moment magnitude), and fault distances from 2 km to 500 km, are simulated. Simulation is performed in magnitude steps of 0.2 units. For each simulated earthquake fault plane, we perform simulations for 25 different locations of the observation point. In order to have a uniform distribution of distances in log units, the distances are 2.2, 3.1, 3.8, 4.4,5.4, 7, 9, 11, 16, 21, 27, 33, 42, 52, 66, 82,103,129, 162, 203, 254, 318, 399, 500 km, where distance is defined as the closest distance from the fault to the observation point. For small earthquakes, the fault distance is equivalent to the hypocentral distance.

Directivity effects, which depend on the azimuth from the fault rupture direction to the observation point, are important for larger earthquakes (Somerville et al., 1987). A complete database should provide data for both backward and forward directivity cases as well as data for azimuths with minimal directivity effects. In order to provide a good simulated database, three profiles for the above-mentioned distances have been considered and are shown in Figure 6. For the backward directivity profile (#1), the hypocenter is located at the

nearest subfault. For the null-directivity profile (#2) the hypocenter is located at the middle of the fault plane. For the forward-directivity profile (#3) the hypocenter is located at the farthest subfault to maximize directivity.

There is little information about the specific fault geometry to be modeled, as Puerto Rico is affected not only by the subduction zone (about 200 km away), but also by many other local faults of unknown location and orientation. Therefore the dip has been considered 90°. The length and width of faults are calculated from the target moment magnitude based on the Wells and Coppersmith (1994) empirical formulas between magnitude and fault size. The sampling rate, near-source shear-wave velocity and density have been considered as 100 sample/sec, 3.6 km/sec and 2.8 g/cm^3 respectively. The attenuation, regional crustal/site amplification and duration models are as given in the previous section (e.g. determined from the empirical data). Based on the calibrated generic source parameters for EXSIM, the source model corresponds to an input stress parameter given by $\Delta\sigma$= 130 bars, with a maximum of 50% of the fault actively pulsing at any moment in time. This is the EXSIM source model that reproduces the California strong-motion database used by Atkinson and Silva (2000) in their stochastic ground-motion model development. A random slip distribution is assumed. High frequency amplitudes are reduced through the kappa operator, which models near surface attenuation, by applying the factor $\exp(-\pi f\kappa)$ (Anderson and Hough 1984). Kappa generally varies between 0.02 and 0.04 for soft rock sites (Anderson and Hough; 1984, Boore et al, 1992; Atkinson and Silva, 1997; Boore and Joyner, 1997). κ= 0.03 is adopted for Puerto Rico as a compromise between regional estimates.

We simulated 1950 acceleration time series for magnitudes from **M**3.0 to **M**8.0 and distances from 2 km to 500 km. The response spectra (pseudoacceleration, PSA, 5% damped) of the simulated time series have been calculated for frequencies from 0.1Hz to 20Hz. Response spectra show the response of a simple oscillator to the time series, and are used in many engineering applications. Figures 7 and 8 show the PSA of the simulated acceleration time series at 0.5 and 5 Hz versus distance for different magnitudes. Each of the three directivity cases is plotted, which results in the observed scatter for each magnitude. We note that this scatter does not represent all contributions to random variability in ground-motion amplitudes, as we have not modeled variability in source parameters or attenuation; the scatter shows directivity effects only. The obtained PSA show a well-behaved trend versus distance.

Comparison of simulated acceleration time series with data

In this section we compare response spectra calculated from simulated records for Puerto Rico with those calculated from actual seismographic records. For a proper comparison we need to have the same type of magnitude for both the simulated time series and the recorded data. The simulated time series are based on moment magnitude, **M.** The reported magnitudes for the real records include

M, mb and local magnitudes based on duration. Thus we first need to obtain the moment magnitudes for the study earthquakes in Puerto Rico.

Based on the Brune point source model, which is appropriate for the small earthquakes of our empirical database, the spectra of the recorded acceleration time series can be modeled using equation 1. The spectra of displacement at low frequencies ($f << f_o$) at a distance of R= 10 km would be; D (f)= $C\mathbf{M_o}$ (using R= 10 km in the constant C; see equation 1). If we play back the attenuation effects (including anelastic and trilinear hinged geometric behaviors) to R= 10 km, then $\mathbf{M_o}$ and hence **M** can be calculated. These calculated moment magnitudes are subjected to significant uncertainty, as they are mostly single-station estimates, based on the records at SJG.

Figures 9-12 show some examples of the distribution of simulated PSA in comparison to PSA from the recorded data. The good agreement between the simulations and records at small to moderate magnitudes, at both low and high frequencies, gives us confidence in our simulation model parameters for Puerto Rico.

Ground-motion relations

Regression analysis is used to obtain ground-motion relations that describe the simulated response spectra as simple functions of magnitude and distance. The maximum likelihood method (Joyner and Boore, 1993) has been applied, for frequencies from 0.1 to 20Hz. The ground-motion relations are for a generic soft rock site condition (assumed NEHRP B or C). The response spectra are fit to

$$\log PSA(f, R) = c_1 + c_2(\mathbf{M}-b) + c_3(\mathbf{M}-b)^n + hingeFunction + c_4(f)R \quad (6)$$

where PSA is the random horizontal-component acceleration response spectra with 5% damping,

M= Moment magnitude

$R = (D^2 + \Delta^2)^{0.5}$

D = closest distance to fault surface, in km

$\Delta = c_5 + c_6\mathbf{M}$

$c_4(f)$= the coefficient of anelastic attenuation

$hingeFunction = (c_7+c_8\mathbf{M})\log(R)$ for $R \leq 75$ km

$hingeFunction = (c_7+c_8\mathbf{M})\log(75)$ for 75 km $< R \leq 100$ km

$hingeFunction = (c_7+c_8\mathbf{M})\log(75) - 0.5\log(R/100)$ for $R > 100$ km

Some of the main seismic sources are located more than 200 km to the north of Puerto Rico. Therefore extending the attenuation formula to large distances is important. The *hingeFunction* defines the hinged behavior of ground-motion curves for different distances.

The maximum likelihood regression algorithm of Joyner and Boore (1993) requires a linear equation for regression. Thus some of the constants must be pre-set to linearize the final regression. Specifically b, n, c_5, c_6, c_7 and c_8 are constants that are pre-set based on initial analysis to determine the best fit and distribution of residuals. Atkinson and Boore (1995, 1997) applied b= 6 and n= 2, while Abrahamson and Silva (1997) applied b= 8.5 and n= 2 or 3. In order to find the best b and n values to set in the source terms, we applied a set of different trial values for both constants to Equation 6. b values from 1 to 10 were considered, while n was varied from 1 to 4. For each pair of b and n the maximum likelihood method was applied to Equation 6 and the average absolute value of residuals for each magnitude for frequencies from 0.1 to 20 Hz were calculated. This analysis showed that the best combination (lowest residuals) is b= 6 and n= 2.

It was determined that a linear relation between **M** and Δ provides a good distributions of residuals. Therefore the parameter space was sampled to find the best linear relation (coefficients c_5 and c_6 that provide the lowest absolute value of residuals). These coefficients control the flat portion of the attenuation relations in the near-source region. The lowest residuals are obtained for the function $\Delta = -7.333 + 2.333\,\mathbf{M}$. Thus we fix c_5= -7.333 and c_6 = 2.333 **M.**

The slope of the attenuation curve as given in *hingeFunction* is magnitude-dependent, with the lowest residuals being obtained for c_7= -1.8 and c_8 = 0.1. The above-mentioned procedures to determine b, n, c_5, c_6, c_7 and c_8 have been iterated many times to find the final values of the parameters which produce the lowest residuals. Therefore equation 6 becomes as follows:

$$\log PSA(f, R) = c1 + c2(\mathbf{M}-6) + c3(\mathbf{M}-6)^2 + hingeFunction + c4(f)R \qquad (7)$$

where PSA is the observed acceleration response spectra with 5% damping

f = frequency in hertz

M = Moment magnitude

$R = (D^2 + \Delta^2)^{0.5}$

D = closest distance to fault surface, in km

$\Delta = -7.333 + 2.333\mathbf{M}$

hingeFunction = $(-1.8 + 0.1\mathbf{M}) \log(R)$ for $R \le 75$ km

hingeFunction = $(-1.8 + 0.1\mathbf{M}) \log(75)$ for 75 km $\le R \le$ 100 km

hingeFunction = $(-1.8 + 0.1\mathbf{M}) \log(75) - 0.5\log(R/100)$ for $R \ge 100$ km

c4(*f*) is the coefficient of anelastic attenuation.

Table 2 shows the final results of maximum likelihood regression analysis of the simulated data to Equation 7. Figures 13-15 show the predicted PSA values by this ground-motion relation (equation 7) in comparison to the simulated PSA values input to the regression. The equations provide a good prediction of the simulated PSA values over all magnitudes and distances, although there is a slight tendency to overestimate near-fault PSA for earthquakes of **M**7 (The curves tend to track the "forward-directivity" or higher of the plotted values for **M**7).

For hazard calculations, we are interested in both the median ground-motion predictions, given by equation (7), and their standard deviation. We calculated the residuals of the recorded Puerto Rico data versus the Puerto Rico attenuation relations (e.g. residual= (log of observed A_{ij}) for real recorded Puerto Rico data – (log of predicted A_{ij}) by equation 7) for our study events. The study events have smaller magnitudes than the range of interest for seismic hazard calculations, but nevertheless serve as a guide to actual variability in the recorded data about the prediction equations. The standard deviation of the distribution of the residuals for intermediate frequencies on average is about 0.28 in log10 units. We suggest a standard deviation of the relations of 0.28 log(10) units for all frequencies. This standard deviation is typical for ground-motion relations in many regions.

Comparison of Puerto Rico ground-motion relations with relations for other regions

In Figures 16 to 19, we compare our ground-motion relations for Puerto Rico with ground-motion relationships for other regions. The other regions are Eastern North America (Atkinson & Boore, 1995), California (Atkinson & Silva, 2000) and the global database for subduction zones (Atkinson & Boore, 2003). The ENA relations of Atkinson and Boore (1995) are based on a stochastic point source model with a two-corner source spectrum to mimic finite fault effects. The California relations are based on a two-corner stochastic source model calibrated against the California strong motion database. The global subduction relations of Atkinson and Boore (2003) are strictly empirical, based on regression analysis of thousands of records; separate regressions were performed for in-slab and interface events. The Atkinson and Boore subduction relations are plotted for **M**7.0 only.

The ground-motion relations for bedrock for ENA have been multiplied by the generic factors of Adams et al. (1999) to convert them from hard rock to a "firm ground" (NEHRP C) site condition. The generic soft rock site condition (NEHRP C) applies for the California relations ("rock" relations of Atkinson & Silva, 2000) and is provided for the global subduction zones (Atkinson & Boore, 2003). Recall that the Puerto Rico curves are assumed to represent soft rock (NEHRP C). The plotted curves are thus comparable to the ground-motion relations of the other regions in terms of site conditions.

The Puerto Rico ground-motion relations are similar to stochastic ground-motion relations obtained for other parts of North America. Differences are attributable to regional variations in ground-motion parameters. There are three main parameters that control the behavior of PSA and which may vary regionally. The first one is the crustal and near-surface amplification. For Puerto Rico this is modeled by the H/V ratio. The other ground-motion relations each represent slightly different overall site effects. Another parameter that controls the behavior of PSA, especially at large distances, is the regional Q-value. At large distances Puerto Rico ground-motion curves lie between those of ENA and California, since the Puerto Rico Q-value is intermediate to those for ENA and California. The third parameter that makes the PSA in Puerto Rico relations deviate from the other relations for North America is differences in the hinge points of the attenuation curve, reflecting regional differences in crustal structure. Overall, the Puerto Rico relations agree well with stochastic relations for California and ENA.

The motions calculated by the global subduction relations of Atkinson and Boore (2003) are quite different from those suggested by this study. The global subduction relations are mostly applicable for **M**>6.0 (interface and in-slab events) and R >40 km (for in-slab events); thus the Puerto Rico PSA should not be compared with the global subduction relations outside these limits. The global subduction relations are entirely empirical. The database of interface events was separated from the database of in-slab events in deriving the empirical regressions. By contrast, the Puerto Rico relations are based on the combination of events of all types. Crustal events have contributions to the Puerto Rico relations as well as interface and in-slab events. Due to the limited data precision for Puerto Rico events, it is not feasible to distinguish between event types in most cases. Thus the Puerto Rico ground motions are region-specific, but the attenuation is averaged over all types of events. By contrast, the global subduction relations separate out event types, but combine data globally over several subduction zones. These factors contribute to the observed differences between global subduction ground-motion relations and Puerto Rico ground-motion relations. For seismic hazard analysis, differences in results obtained using global empirical relations, in comparison to those obtained using the region-specific relations presented here, are a measure of our current level of uncertainty.

Conclusion

We derived the first region-specific ground-motion relations for Puerto Rico, based on evaluation of regional seismographic data from small to moderate earthquakes, coupled with application of a stochastic simulation model to extend the data to larger magnitudes. The relations are in good agreement with recorded ground-motion data in Puerto Rico, and are intermediate to relations for California and Eastern North America. Future study is required to address such factors as the effect of event type (crustal, interface or in-slab) on ground motions, and to improve the knowledge of regional site effects.

Acknowledgments

This study was supported by the U.S. National Earthquake Hazards Reduction Program. We thank Christa von Hillebrandt, Martinez Cruzado and PRSN staff for their effort to provide seismic data and their help to calibrate the PRSN seismic network. We thank Igor Beresnev for stimulating discussion and comments on finite fault modeling. The comments of Bill McCann, Roland Laforge, Art Frankel and Chuck Mueller are also gratefully acknowledged.

References

Abrahamson, N. and W. Silva (1997). Empirical response spectral attenuation relations for shallow crustal earthquakes. Seism. Res. L., **68**, 94-127.

Adams, J., Weichert, D. H , and Stephen Halchuk (1999) Trial Seismic Hazard Maps of Canada - 1999: 2%/50 Year Values for Selected Canadian Cities, Geological Survey of Canada Open File 3724.

Aki, K. (1967). Scaling law of seismic spectrum, J. Geophys. Res. 72, 1217-1231.

Anderson, J. and S. Hough (1984). A model for the shape of the Fourier amplitude spectrum of acceleration at high frequencies. Bull. Seism. Soc. Am., **74**, 1969-1993.

Atkinson, G. (1995). Ground motion relations in eastern North America. Proc. Atomic Energy Control Board Workshop on Seismic Hazards, June 21-23, Ottawa.

Atkinson, G., and D. Boore (1995). New ground motion relations for eastern North America. Bull. Seism. Soc. Am., **85**, 17-30.

Atkinson, G., and D. Boore (1997). Stochastic point-source modeling of ground motions in the Cascadia region. Seism. Res. L., **68**, 74-85.

Atkinson, G. and D. Boore (1997). Some comparisons of recent ground motion relations. Seism. Res. L., **68**, 24-40.

Atkinson, G. and D. Boore (1998). Evaluation of models for earthquake source spectra in eastern North America. Bull. Seism. Soc. Am., **88**, 917-934.

Atkinson, G. and D. Boore (2002). Empirical ground motion relation for subduction zone earthquakes. Bull. Seism. Soc. Am., submitted.

Atkinson, G. and J. Cassidy (2000). Integrated use of seismograph and strong motion data to determine soil amplification in the Fraser Delta: results from the Duvall and Georgia Strait earthquakes. Bull. Seism. Soc. Am., **90**, 1028-1040..

Atkinson, G. and R. Mereu (1992). The shape of ground motion attenuation curves in southeastern Canada. Bull. Seism. Soc. Am., **82**, 2014-2031.

Atkinson, G. and W. Silva (1997). Empirical source spectra for California earthquakes. Bull. Seism. Soc. Am., **87**, 97-113.

Atkinson, G. and W. Silva (2000). Stochastic modeling of California ground motions. Bull. Seism. Soc. Am., **90**, 255-274.

Beresnev, I. and G. Atkinson (1997). Modeling finite fault radiation from the w^n spectrum. Bull. Seism. Soc. Am., **87**, 67-84.

Beresnev, I. and G. Atkinson (1998a). Stochastic finite-fault modeling of ground motions from the 1994 Northridge, California earthquake. I. Validation on rock sites. Bull. Seism. Soc. Am., **88**, 1392-1401.

Beresnev, I. and G. Atkinson (1998b). FINSIM - a FORTRAN program for simulating stochastic acceleration time histories from finite faults. Seism. Res. L., **69**, 27-32.

Beresnev, I. and G. Atkinson (1999). Generic finite-fault model for ground-motion prediction in eastern North America. Bull. Seism. Soc. Am., **89**, 608-625.

Beresnev, I. and G. Atkinson (2000). Subevent structure of large earthquakes – A ground motion perspective. Geophys. Res. L., **28**, 53-56.

Beresnev, I. and G. Atkinson (2001). Source parameters of earthquakes in eastern and western North America based on finite-fault modeling. Bull. Seism. Soc. Am., **91**, submitted.

Boore, D. (1983). Stochastic simulation of high-frequency ground motions based on seismological models of the radiated spectra. Bull. Seism. Soc. Am., **73**, 1865-1894.

Boore, D. and G. Atkinson (1987). Stochastic prediction of ground motion and spectral response parameters at hard-rock sites in eastern North America. Bull. Seism. Soc. Am., **77**, 440-467.

Boore, D. and W. Joyner (1997). Site amplifications for generic rock sites. Bull. Seism. Soc. Am., **87**, 327-341.

Boore, D. W. Joyner and T. Fumal (1997). Equations for estimating horizontal response spectra and peak acceleration from western North American earthquakes: A summary of recent work. Seism. Res. L., **68**, 128-153

Boore, D., W. Joyner and L. Wennerberg (1992). Fitting the stochastic omega-squared source model to observed response spectra in western North America: trade-offs between stress drop and kappa. Bull. Seism. Soc. Am., **82**, 1956-1963.

Borcherdt, R. (1995). Estimates of site-dependent response spectra for design. Earthquake Spectra, **10**, 617-654.

Brune, J. (1970). Tectonic stress and the spectra of seismic shear waves from earthquakes. J. Geophys. Res., **75**, 4997-5009.

Brune, J. (1971). Correction. J. Geophys. Res., 76, 5002.

Chen, S. (2000). Global comparisons of earthquake source spectra. Ph.D. Thesis, Carleton University, Earth Science dept.

Chen, S. and G. Atkinson (2002). Global comparisons of earthquake source spectra. Bull. Seism. Soc. Am., **92,** 885-895.

Hanks, T. and R. McGuire (1981). The character of high-frequency strong ground motion. Bull. Seism. Soc. Am., **71**, 2071-2095.

Hartzell, S. (1978). Earthquake aftershocks as Green's functions. Geophys. Res. Letters, **5**, 1-14.

Heaton, T., and S. Hartzell (1986). Source characteristics of hypothetical subduction earthquakes in the Northwestern United States. Bull. Seism. Soc. Am., **76**, 675-708.

Irikura, K. (1983). Semi-empirical estimation of strong ground motions during large earthquakes. Bull. Disaster Prevention Res. Inst., Kyoto Univ., **33**, 63-104.

Joyner, W. and D. Boore (1986). On simulating large earthquakes by Green's function additon of smaller earthquakes. In: Earthquake Source Mechanics. Maurice Ewing Volume 6. Geophys. Monogr. Am. Geophys. Union, **37**, 269-274.

Joyner, W. and D. Boore (1993). Methods for regression analysis of strong motion data. Bull. Seism. Soc. Am., **83**, 469-487.

Lermo, J. and F. Chavez-Garcia (1993). Site effect evaluation using spectral ratios with only one station. Bull. Seism. Soc. Am., **83**, 1574-1594.

McCann, W., 1985, On the Earthquake Hazard of Puerto Rico and the Virgin Islands, Bull. Seism. Soc. Am., 75, 251-262.

McCann, W. R., 2002a, Catalog of Felt Earthquakes for Puerto Rico and Neighboring Islands 1492-1900 with Additional Information for Some 20th Century Earthquakes, in prep.

Nakamura, Y. (1989). A method for dynamic characteristics estimation of subsurface using microtremor on the ground surface. QR RTRI **30**, 25-33.

Raoof, M., R. Herrmann and L. Malagnini (1999). Attenuation and excitation of three-component ground motion in sourthern California. Bull.Seism. Soc. Am., **89**, 888-902.

Sadigh, K., C. Chang, J. Egan, F. Makdisi and R. Youngs (1997). Attenuation relationships for shallow crustal earthquakes based on California strong motion data. Seism. Res. L., **68**, 180-189.

Shin, T. and R. Herrmann (1987). Lg attenuation and source studies using 1982 Miramichi data. Bull Seism. Soc. Am., 77, 384-397.

Somerville, P., M. Sen and B. Cohee (1991). Simulations of strong ground motions recorded during the 1985 Michoacan, Mexico and Valparaiso, Chile, earthquakes. Bull. Seism. Soc. Am., **81**, 1-27.

Somerville., P., Smith N.C., and Graves, R.W. (1997). Modification of Empirical Strong Ground Motion Attenuation Relations to Include the Amplitude and Duration Effects of Rupture Directivity. Seismological Research Letter, 68, number 1, 199-221.

Toro, G., N. Abrahamson and J. Schneider (1997). Model of strong ground motion in eastern and central North America: Best estimates and uncertainties. Seism. Res. L., **68**, 41-57.

Tumarkin, A. and R. Archuleta (1994). Empirical ground motion prediction. Annali Di Geofisica. 37, 1691-1720..

Wells, D. and K. Coppersmith (1994). New empirical relationships among magnitude, rupture length, rupture width, rupture area, and surface displacement. Bull. Seism. Soc. Am., **84**, 974-1002.

Zeng, Y., J. Anderson and G. Yu (1994). A composite source model for computing realistic synthetic strong ground motions. Geophys. Res. L., in press.

Appendix A: EXSIM, a stochastic finite fault modeling program introducing the concept of dynamic corner frequency

The stochastic model is a commonly used tool for ground motion simulation. The method models ground motion as band limited Gaussian noise, whose amplitude spectrum is given by a seismological model (Boore, 1983). The most commonly-used seismological model for stochastic simulations has been the Brune (1970, 1971) point source model (e.g. Toro et al., 1997), However, point source models are inappropriate for large earthquakes. The effects of a large finite source, including fault geometry, heterogeneity of slip on the fault plane and directivity, can profoundly influence the amplitudes, frequency content and duration of ground motion. Finite-fault effects in ground motions become important for earthquakes with magnitudes exceeding approximately 6.0.

Finite fault modeling has been an important tool for the prediction of ground motion near the epicenters of large earthquakes (Hartzel, 1978; Irikura, 1983; Joyner and Boore, 1986; Heaton and Hartzel, 1986; Somerville et al., 1991; Tumarkin and Archuleta, 1994; Zeng et al., 1994; Beresnev and Atkinson, 1998a). One of the most useful methods to simulate ground motion for a large earthquake is based on the simulation of a number of small earthquakes as subfaults that comprise a big fault. A large fault is divided into N subfaults and each subfault is considered as a small point source (introduced by Hartzel, 1978). The rupture spreads radially from the hypocenter. In our implementation, the ground motions of subfaults, each of which are calculated by the stochastic point-source method, are summed with a proper delay time in the time domain to obtain the ground motion from the entire fault, a(t):

$$a(t)= \sum_{i=1}^{nl} \sum_{j=1}^{nw} a_{ij}(t+\Delta t_{ij}) \qquad (1)$$

where *nl* and *nw* are the number of subfaults along the length and width of main fault, respectively ($nl*nw = N$), Δt_{ij} is the relative delay time for the radiated wave from the ij^{th} subfault to reach the observation point. The $a_{ij}(t)$ are each calculated by the stochastic point source method. The acceleration spectrum for a subfault at a distance R_{ij} is modeled as a point source with an ω^2 shape (Aki, 1967; Brune, 1970; Boore 1983). The acceleration spectrum of shear wave of the ij^{th} subfault, $A_{ij}(f)$, is:

$$A_{ij}(f)=CM_{0ij}(2\pi f)^2/[1+(f/f_{0ij})^2]\exp(-\pi f\kappa)\exp(-\pi f R/Q\beta)/R_{ij} \qquad (2)$$

where M_{0ij} , f_{0ij} and R_{ij} are the ij^{th} subfault seismic moment, corner frequency and distance from the observation point, respectively. Corner frequency, f_{0ij} , is given by $f_{0ij}=4.9e+6\,\beta\,(\Delta\sigma / M_{0ij})^{1/3}$ where $\Delta\sigma$ is stress drop in bars M_{0ij} is in dyne-cm and β is shear wave velocity in km/s. The constant $C=4\pi^2\Re^{\theta\varphi}/4\pi\rho\beta^3R_{ij}$, where ρ=density and $\Re^{\theta\varphi}$ = radiation pattern (Boore, 1983). exp $(-\pi f\kappa)$ is a high

cut filter to model near-surface "*kappa*" effects: this is the commonly-observed rapid spectral decay at high frequencies. The quality factor, *Q*, is inversely related to anelastic attenuation.

The moment of each subfault is controlled by the ratio of its area to the area of the main fault ($M_{oij}=M_o/N$ where M_0 is the seismic moment of the entire fault). If the subfaults are not identical we can express the seismic moment of each subfault as:

$$M_{oij} = (M_o S_{ij})/(\sum_{l=1}^{nl} \sum_{k=1}^{nw} S_{kl}) \qquad (3)$$

where S_{ij} is the relative slip weight of the ij^{th} subfault. Earthquake time history simulation deals with the time from the beginning of rupture to the time when the rupture stops. In our finite fault model we deal with a ruptured area that is time dependent; it is initially zero and is finally equal to the entire fault area. Corner frequency is inversely proportional to the ruptured area. Therefore in time history simulation the corner frequency may be considered as a function of time. The rupture begins with high corner frequencies and progresses to lower corner frequencies. We suppose that, during an earthquake, at each moment of time the corner frequency is dependent on the cumulative ruptured area. The rupture history controls the frequency content of the simulated time series.

In our dynamic approach, the corner frequency of the first subfault (near the beginning of rupture) is $f_{011}=S\ 4.9e+6\ \beta\ (\Delta\sigma / M_{011})^{1/3}$, where M_{011} is the seismic moment of the first subfault. The dynamic corner frequency of the ij^{th} subfault, $f_{oij}(t)$, can be defined as a function of $N_R(t)$, the cumulative number of ruptured subfaults at time t.

$$f_{oij}(t)= N_R(t)^{-1/3}\ S\ 4.9e+6\ \beta\ (\Delta\sigma / M_{oave})^{1/3} \qquad (4)$$

where $M_{oave} = M_o/ N$ is the average seismic moment of subfaults and *S* is a constant. As the rupture proceeds towards the end of the fault the number of ruptured subfaults increases and, based on equation 4, the corner frequency of the subfaults decreases. The dynamic corner frequency concept will tend to decrease the high-frequency level of the spectrum of subfaults as the rupture progresses ($A_{ij}(f)_{f>>fijo} \propto f_{oij}^2$). We therefore introduce a scaling factor to conserve the high-frequency spectral level of the radiation produced by each subfault. The acceleration spectrum of the ij^{th} subfault, $A_{ij}(f)$, is thus:

$$A_{ij}(f)=C\ M_{oij}\ H\ f^2 /[1+(f/f_{oij})^2] \qquad (5)$$

$$H = (N\int \{f^2/ [1+(f/ f_0)^2]\}^2\ df /\int \{ f^2/ [1+(f/f_{oij})^2]\}^2\ df)^{1/2} \qquad (6)$$

where *H* is the scaling factor. Thus the diminishing effect of f_{oij} on the high-frequency spectral level from the subfault is compensated for by the scaling factor. The high-frequency spectral contribution from the ij^{th} subfault is equal to

that from the first subfault, but the calculation of corner frequency, which controls the shape of the spectrum, comes from the total ruptured area. Consequently, as the rupture progresses there is more low-frequency energy produced, and thus the distribution of energy tends to shift towards lower frequencies.

The new simulation approach is implemented in a modified version of the computer program FINSIM (Beresnev and Atkinson, 1998b). FINSIM is a well-known stochastic finite-fault simulation program that has been validated using data from many earthquakes, including Michoacan, Mexico (1985); Lama Prieta (1989); Northridge (1994); Valparaiso, Chile (1985); and Saguenay, Quebec (1988) (Beresnev and Atkinson 1997, 1998a, 1998b, 1999, 2000, 2001). The modified program has been renamed EXSIM. The modifications include the following features.

- Inclusion of the new concept of "dynamic corner frequency"
- Elimination of multiple triggering of subfaults.
- Variability of pulsing area, or the number of subfaults which are considered as active subfaults in the calculation of dynamic corner frequency. This allows for self-healing slip models.
- Calculation of subfault seismic moment based on dividing the total seismic moment of the earthquake fault by the number of subfaults.

In EXSIM the percentage of pulsing area on the fault will affect the relative amplitudes of low-frequency motion in finite fault modeling. Variation of the stress drop parameter can be used to adjust the relative amplitudes of high-frequency motion. By increasing the stress parameter, the amplitude of high frequencies increases.

A generic EXSIM model was derived by finding the model parameters which best reproduce, on average, the California strong-motion database (as used by Atkinson and Silva, 2000). For this exercise, the regional attenuation parameters used in previous finite-fault simulations for California were adopted (Beresnev and Atkinson, 2001), and the calibration exercise determined the best-fit stress drop and pulsing percentage. These parameters were found to be independent of magnitude, with average values of $\Delta\sigma$ = 130 bars and a pulsing percentage of 50%. EXSIM produces similar results to FINSIM over the magnitude range from 5.5 to 7.5, but unlike FINSIM it can be easily extended to smaller magnitudes. The advantage of EXSIM is that it introduces conceptual improvements, such as independence of results from subfault size and conservation of radiated energy, and allows simulation of self-healing slip pulses.

References

Aki, K. (1967). Scaling law of seismic spectrum, J. Geophys. Res. 72, 1217-1231.

Beresnev, I. and G. Atkinson (1997). Modeling finite fault radiation from the w^n spectrum. Bull. Seism. Soc. Am., **87**, 67-84.

Beresnev, I. and G. Atkinson (1998a). Stochastic finite-fault modeling of ground motions from the 1994 Northridge, California earthquake. I. Validation on rock sites. Bull. Seism. Soc. Am., **88**, 1392-1401.

Beresnev, I. and G. Atkinson (1998b). FINSIM - a FORTRAN program for simulating stochastic acceleration time histories from finite faults. Seism. Res. L., **69**, 27-32.

Beresnev, I. and G. Atkinson (1999). Generic finite-fault model for ground motion prediction in eastern North America. Bull. Seism. Soc. Am., **89**, 608-625.

Beresnev, I. and G. Atkinson (2000). Subevent structure of large earthquakes – a ground motion perspective. Geophys. Res. L.,**28**, 53-56.

Beresnev, I. and G. Atkinson (2001). Source parameters of earthquakes in eastern and western North America based on finite-fault modeling. Bull. Seism. Soc. Am., **91**, submitted.

Boore, D. (1983). Stochastic simulation of high-frequency ground motions based on seismological models of the radiated spectra. Bull. Seism. Soc. Am., **73**, 1865-1894.

Brune, J. (1970). Tectonic stress and the spectra of seismic shear waves from earthquakes. J. Geophys. Res., **75**, 4997-5009.

Brune, J. (1971). Correction. J. Geophys. Res., 76, 5002.

Hartzell, S. (1978). Earthquake aftershocks as Green's functions. Geophys. Res. Letters, **5**, 1-14.

Heaton, T., and S. Hartzell (1986). Source characteristics of hypothetical subduction earthquakes in the Northwestern United States. Bull. Seism. Soc. Am., **76**, 675-708.

Irikura, K. (1983). Semi-empirical estimation of strong ground motions during large earthquakes. Bull. Disaster Prevention Res. Inst., Kyoto Univ., **33**, 63-104.

Joyner, W. and D. Boore (1986). On simulating large earthquakes by Green's function additon of smaller earthquakes. In: Earthquake Source Mechanics. Maurice Ewing Volume 6. Geophys. Monogr. Am. Geophys. Union, **37**, 269-274.

Somerville, P., M. Sen and B. Cohee (1991). Simulations of strong ground motions recorded during the 1985 Michoacan, Mexico and Valparaiso, Chile, earthquakes. Bull. Seism. Soc. Am., **81**, 1-27.

Toro, G., N. Abrahamson and J. Schneider (1997). Model of strong ground motion in eastern and central North America: Best estimates and uncertainties. Seism. Res. L., **68**, 41-57.

Tumarkin, A. and R. Archuleta (1994). Empirical ground motion prediction. Annali Di Geofisica. 37, 1691-1720.

Zeng, Y., J. Anderson and G. Yu (1994). A composite source model for computing realistic synthetic strong ground motions. Geophys. Res. L., in press.

Table 1. Earthquakes used in this study

	Date			Time	LAT.	LONG.	DEPTH (km)	catalogue		Moment
	Y	M	D	h				Magnitude		Magnitude
1	1993	7	22	20	18.58	-69.00	109	4.8	mb	4.5
2	1993	8	1	19	17.40	-65.72	25	5.3	Mw	5.3
3	1993	8	10	7	19.35	-64.89	36	4.5	mb	4.3
4	1993	9	30	0	18.75	-62.80	33	4.3	mb	3.5
5	1993	10	3	13	17.80	-62.75	10	4.2	Md	3.8
6	1993	10	18	9	18.66	-64.45	30	4.3	mb	4.0
7	1993	10	24	17	19.68	-70.38	33	4.0	mb	4.1
8	1993	11	5	2	19.02	-66.01	48	4.9	mb	4.4
9	1993	11	8	3	19.20	-68.08	10	4.6	mb	4.1
10	1994	1	6	17	18.05	-68.37	87	4.0	mb	4.2
11	1994	1	8	22	18.22	-64.33	103	4.8	mb	4.6
12	1994	1	13	20	18.84	-66.18	47	4.0	mb	3.7
13	1994	1	18	12	18.58	-68.82	163	4.6	mb	4.3
14	1994	1	21	18	19.67	-64.43	10	4.0	mb	3.8
15	1994	2	25	16	19.25	-64.23	33	4.3	mb	4.2
16	1994	2	25	17	19.25	-64.33	32	4.9	mb	4.7
17	1994	3	1	18	19.39	-65.16	10	4.3	mb	4.1
18	1994	3	10	3	17.81	-65.35	10	4.1	mb	3.8
19	1994	4	21	17	18.00	-62.88	75	5.0	mb	4.8
20	1994	5	1	4	17.93	-64.70	162	4.3	mb	3.9
21	1994	6	25	6	19.01	-66.83	46	4.7	mb	4.3
22	1994	6	25	8	18.94	-66.68	33	4.0	Md	3.4
23	1994	7	11	3	19.23	-66.76	10	4.4	mb	4.1
24	1994	7	17	23	17.63	-62.94	131	4.2	mb	4.0
25	1994	9	23	23	18.43	-61.53	31	4.4	Md	4.3
26	1994	10	12	3	18.24	-68.37	107	4.4	mb	4.3
27	1994	11	17	3	17.92	-68.69	33	4.5	mb	4.3
28	1994	11	17	14	18.62	-68.34	81	4.7	mb	4.7
29	1994	11	30	2	19.53	-64.60	19	4.5	mb	4.5
30	1995	1	1	9	19.22	-69.42	42	4.8	mb	4.9
31	1995	1	18	20	18.89	-70.33	91	5.0	mb	5.1
32	1995	2	1	10	18.19	-68.36	179	4.6	mb	4.7
33	1995	2	16	11	18.88	-64.18	33	4.1	mb	4.3
34	1995	2	16	14	19.48	-65.79	33	4.0	mb	4.3
35	1995	5	4	20	18.89	-64.29	47	4.5	Md	4.3
36	1995	6	20	13	17.88	-62.85	100	4.2	mb	4.3
37	1995	7	9	18	19.62	-67.14	33	4.6	mb	4.1
38	1995	7	26	9	19.19	-64.67	52	4.6	mb	4.5
39	1995	7	28	0	19.57	-69.62	33	4.2	mb	4.3
40	1995	8	13	9	19.41	-69.36	10	4.4	mb	4.3
41	1995	9	19	3	18.79	-62.53	10	4.7	mb	4.1
42	1995	10	8	4	19.01	-66.96	46	4.8	Md	4.4
43	1995	10	31	1	19.70	-69.75	62	4.8	mb	4.2

44	1995	12	9	5	18.89	-65.71	50	4.2	mb	3.8
45	1995	12	31	0	18.44	-64.60	33	4.7	Ml	4.2
46	1996	1	2	18	18.79	-62.70	33	4.5	Ml	3.9
47	1996	1	24	1	18.19	-69.99	50	4.4	mb	4.1
48	1996	3	20	12	19.22	-66.75	33	4.1	mb	3.9
49	1996	4	9	19	18.88	-69.72	88	4.1	mb	4.2
50	1996	5	11	2	19.31	-64.96	35	5.1	Mw	5.1
51	1996	5	12	4	18.48	-63.84	33	4.7	mb	4.4
52	1996	5	14	11	18.94	-65.08	33	4.2	mb	3.9
53	1996	5	29	11	18.06	-69.64	52	4.0	mb	4.1
54	1996	6	11	16	17.25	-68.28	33	5.5	mb	4.7
55	1996	6	12	3	20.03	-70.19	33	4.5	mb	4.3
56	1996	7	21	9	18.30	-62.41	60	4.5	mb	4.2
57	1996	10	17	17	19.02	-69.11	33	4.4	mb	4.3
58	1996	11	1	1	18.60	-64.28	33	4.4	mb	3.8
59	1996	11	6	2	18.85	-64.32	21	5.1	mb	4.7
60	1996	11	8	7	18.04	-68.53	73	4.8	mb	4.5
61	1996	12	4	19	19.04	-69.26	108	4.2	mb	4.3
62	1997	2	24	4	19.32	-69.23	90	4.5	mb	4.1
63	1997	3	17	5	19.01	-62.84	33	5.5	Mw	5.5
64	1997	4	5	21	19.08	-63.12	33	4.3	mb	4.0
65	1997	5	14	2	19.63	-70.29	54	4.7	mb	4.7
66	1997	7	30	16	18.00	-70.32	10	4.9	mb	4.1
67	1997	10	12	15	18.58	-66.22	100	3.7	Md	3.3
68	1997	10	15	19	18.67	-67.44	10	3.3	Md	3.5
69	1997	10	24	0	17.99	-65.31	5	3.2	Md	3.1
70	1997	11	2	11	19.24	-66.34	33	4.3	mb	4.1
71	1997	11	21	7	18.56	-67.01	100	3.2	Md	3.2
72	1997	12	6	17	18.75	-67.34	80	3.5	Md	3.2
73	1997	12	21	2	18.58	-66.54	80	3.1	Md	3.0
74	1997	12	26	0	18.18	-68.44	94	4.7	mb	4.3
75	1997	12	27	13	17.82	-66.10	5	3.0	Md	2.8
76	1997	12	31	3	17.84	-66.10	10	3.0	Md	2.8
77	1997	12	31	21	18.50	-66.13	100	3.1	Md	3.2
78	1998	1	16	12	18.55	-66.12	106	3.1	Md	3.0
79	1998	1	17	23	18.96	-64.61	72	3.5	Md	3.3
80	1998	1	18	14	19.17	-64.66	25	4.4	mb	4.0
81	1998	1	18	13	18.98	-64.64	52	3.6	Md	3.3
82	1998	1	19	22	18.20	-67.17	13	3.7	Md	3.3
83	1998	1	20	12	19.03	-65.09	97	3.5	Md	3.3
84	1998	2	13	3	19.09	-66.09	27	3.0	Md	3.1
85	1998	2	13	18	18.05	-65.46	14	3.7	Md	3.3
86	1998	2	18	16	18.37	-64.97	24	3.3	Md	3.1
87	1998	2	19	5	19.15	-66.43	37	3.0	Md	3.1
88	1998	3	5	7	20.01	-63.15	33	5.1	Mw	5.1
89	1998	3	10	23	18.04	-65.60	1	3.2	Md	3.0
90	1998	3	12	6	18.14	-66.70	60	3.5	Md	3.3
91	1998	3	19	1	18.86	-66.02	56	3.1	Md	3.1
92	1998	3	25	8	19.38	-67.09	25	4.9	mb	4.4
93	1998	3	27	3	18.66	-64.25	50	3.4	Md	3.4
94	1998	4	1	6	18.15	-67.34	0	3.1	Md	3.1

95	1998	4	10	12	18.15	-66.85	16	3.0	Md	2.9
96	1998	4	15	6	18.18	-64.20	25	3.5	Md	3.3
97	1998	4	15	17	17.92	-65.54	2	3.8	Md	3.5
98	1998	4	16	18	17.78	-65.61	2	3.1	Md	3.1
99	1998	4	16	20	18.02	-65.63	0	3.6	Md	3.0
100	1998	4	16	22	18.07	-65.54	0	3.0	Md	2.9
101	1998	4	17	6	19.08	-67.36	22	3.1	Md	3.2
102	1998	4	18	9	18.65	-67.49	1	3.6	Md	3.3
103	1998	4	20	15	18.67	-66.72	79	3.4	Md	3.1
104	1998	4	25	5	19.00	-67.49	25	3.3	Md	3.2
105	1998	4	26	10	18.22	-67.09	20	3.6	Md	3.1
106	1998	4	26	14	19.07	-66.41	30	3.3	Md	3.0
107	1998	4	29	15	18.16	-65.87	87	3.8	Md	3.5
108	1998	4	30	0	18.71	-65.04	71	3.2	Md	3.2
109	1998	5	12	4	18.04	-65.55	0	3.1	Md	2.8
110	1998	5	14	6	17.95	-64.67	25	3.6	Md	3.2
111	1998	5	15	21	19.14	-66.49	49	3.5	Md	3.3
112	1998	5	22	4	19.22	-66.70	36	3.8	Md	3.4
113	1998	5	24	5	19.11	-67.17	25	3.6	Md	3.2
114	1998	5	27	19	19.23	-66.65	24	3.7	Md	3.4
115	1998	5	29	15	19.66	-66.95	10	3.6	Md	3.5
116	1998	6	8	11	18.19	-66.54	66	3.6	Md	3.2
117	1998	6	13	4	17.75	-64.14	30	3.6	Md	3.3
118	1998	6	13	9	19.48	-66.36	48	3.9	Md	3.4
119	1998	6	14	13	18.62	-65.27	48	3.9	Md	3.5
120	1998	6	18	22	18.08	-65.53	0	3.3	Md	2.9
121	1998	6	21	2	18.97	-64.30	58	3.6	Md	3.4
122	1998	6	23	19	19.42	-65.28	49	3.8	Md	3.5
123	1998	6	24	22	17.74	-66.33	17	3.6	Md	3.2
124	1998	6	25	4	18.68	-65.99	68	3.1	Md	3.1
125	1998	7	4	23	18.32	-65.95	135	3.7	Md	3.1
126	1998	7	5	7	18.85	-67.23	18	3.0	Md	3.0
127	1998	7	19	9	18.30	-65.10	131	4.6	mb	4.2
128	1998	7	25	22	19.12	-66.11	15	3.1	Md	3.2
129	1998	7	27	1	18.71	-66.51	25	3.1	Md	3.1
130	1998	7	28	8	18.69	-65.00	25	3.3	Md	3.2
131	1998	8	2	2	18.84	-67.27	13	3.1	Md	3.1
132	1998	8	3	21	18.61	-67.44	12	3.3	Md	3.2
133	1998	8	4	15	19.23	-64.66	60	3.8	Md	3.8
134	1998	8	4	21	19.13	-64.51	56	3.6	Md	3.3
135	1998	8	5	23	19.23	-64.66	60	3.7	Md	3.7
136	1998	8	8	7	18.01	-66.61	13	3.0	Md	2.8
137	1998	8	9	11	19.74	-70.00	33	4.5	mb	4.0
138	1998	8	9	21	18.97	-64.93	22	3.5	Md	3.2
139	1998	8	9	23	18.85	-64.55	95	3.6	Md	3.4
140	1998	8	10	21	18.65	-70.54	58	5.2	Mw	5.2
141	1998	8	10	0	19.16	-64.77	72	3.7	Md	3.5
142	1998	8	10	8	19.30	-64.74	25	3.6	Md	3.3
143	1998	8	11	6	19.21	-66.14	25	3.0	Md	3.0
144	1998	8	26	10	18.75	-65.99	69	3.6	Md	3.3
145	1998	8	30	20	18.69	-70.27	33	4.2	mb	4.0

146	1998	9	2	8	17.96	-66.34	9	3.3	Md	2.8
147	1998	9	3	15	17.94	-66.33	8	3.2	Md	2.7
148	1998	9	12	4	17.94	-66.32	6	3.2	Md	2.7
149	1998	10	10	2	18.25	-66.29	6	3.2	Md	2.6
150	1998	10	15	21	18.49	-70.47	68	4.4	mb	4.4
151	1998	10	15	4	18.86	-65.16	53	3.6	Md	3.2
152	1998	10	18	0	17.96	-65.68	5	3.2	Md	2.9
153	1998	10	22	7	18.92	-65.14	59	3.6	Md	3.4
154	1998	10	23	18	18.87	-64.38	33	4.0	Md	3.7
155	1998	10	23	19	19.50	-64.55	65	3.8	Md	3.9
156	1998	10	24	1	18.86	-64.32	56	4.6	mb	4.2
157	1998	10	24	14	18.62	-66.73	19	3.4	Md	3.0
158	1998	10	29	4	18.20	-65.94	14	3.0	Md	2.7
159	1998	11	1	21	19.04	-65.23	45	3.6	Md	3.3
160	1998	11	1	22	19.14	-65.13	67	3.6	Md	3.4
161	1998	11	3	19	18.84	-65.07	25	3.4	Md	3.1
162	1998	11	4	2	18.75	-65.93	73	3.1	Md	3.0
163	1998	11	9	5	19.30	-65.25	75	3.7	Md	3.4
164	1998	11	11	8	18.24	-67.04	17	3.9	Md	3.4
165	1998	11	15	0	18.82	-66.25	35	3.1	Md	3.0
166	1998	11	16	12	18.90	-67.38	58	3.1	Md	3.1
167	1998	11	21	1	18.84	-65.23	72	3.1	Md	3.2
168	1998	11	23	7	18.72	-66.12	25	3.1	Md	2.9
169	1998	11	24	6	19.14	-67.78	33	4.4	mb	4.1
170	1999	1	18	19	18.86	-67.22	33	5.0	Mw	5.0
171	1999	1	25	10	16.89	-62.50	140.3	4.6	mb	4.0
172	1999	1	25	17	19.50	-66.69	50.1	4.6	mb	4.0
173	1999	1	27	12	18.94	-63.26	33	4.1	mb	4.2
174	1999	4	20	5	18.58	-65.37	91.8	4.2	mb	3.6
175	1999	8	5	15	18.88	-67.18	71.6	4.3	mb	4.0
176	1999	8	7	12	18.76	-66.86	63.4	4.5	mb	4.1
177	1999	10	28	12	18.72	-67.25	33	4.1	mb	3.8
178	1999	12	20	10	17.31	-61.71	58.8	5.4	mb	5.0
179	2000	1	6	11	18.26	-68.32	178	4.0	Md	3.8
180	2000	1	9	2	17.94	-67.00	28	3.1	Md	3.4
181	2000	1	9	5	18.77	-67.25	68	3.2	Md	3.2
182	2000	1	13	18	18.97	-66.58	45	3.1	Md	3.0
183	2000	1	14	6	18.14	-67.91	131	3.4	Md	3.4
184	2000	1	18	11	17.93	-65.66	4	3.1	Md	2.9
185	2000	1	18	23	18.93	-68.10	10	3.8	Md	3.4
186	2000	1	22	12	18.63	-66.88	12	3.0	Md	2.8
187	2000	1	25	14	19.61	-68.06	69	4.1	Md	3.7
188	2000	1	26	15	19.00	-67.76	34	3.0	Md	3.2
189	2000	1	29	3	18.89	-64.30	50	4.4	mb	4.1
190	2000	2	2	9	18.28	-66.23	74	3.0	Md	2.9
191	2000	2	3	11	19.17	-66.52	9	3.6	Md	3.2
192	2000	2	4	0	19.48	-68.05	15	3.7	Md	3.4
193	2000	2	4	23	17.86	-67.04	28	3.2	Md	3.1
194	2000	2	6	21	17.99	-65.55	4	3.1	Md	2.9
195	2000	2	9	4	18.69	-67.52	2	3.5	Md	3.3
196	2000	2	10	4	18.07	-65.86	7	3.8	Md	3.3

197	2000	2	21	16	18.32	-67.88	108	4.4	mb	4.0
198	2000	2	26	12	18.93	-65.90	76	3.9	Md	3.3
199	2000	2	27	23	17.83	-60.99	16	5.0	Md	4.6
200	2000	3	2	14	18.89	-65.18	42	3.7	Md	3.3
201	2000	3	5	6	18.91	-66.85	10	3.2	Md	2.9
202	2000	3	5	16	19.04	-66.86	40	3.3	Md	2.9
203	2000	3	5	20	18.95	-66.91	46	3.0	Md	3.0
204	2000	3	6	1	18.89	-66.40	46	3.0	Md	2.9
205	2000	3	6	2	18.13	-66.92	13	3.2	Md	3.1
206	2000	3	8	2	18.08	-67.11	18	3.0	Md	2.9
207	2000	3	8	9	19.16	-66.48	41	3.6	Md	3.1
208	2000	3	9	0	17.83	-65.66	8	3.4	Md	2.9
209	2000	3	14	18	18.01	-67.07	5	3.5	Md	3.1
210	2000	3	15	9	19.72	-66.04	72	3.9	Md	3.5
211	2000	3	20	15	18.41	-66.62	119	3.9	Md	3.7
212	2000	3	22	2	18.52	-67.56	9	3.0	Md	3.2
213	2000	3	25	7	19.58	-68.15	25	3.8	Md	3.4
214	2000	3	25	13	19.26	-67.55	14	3.4	Md	3.3
215	2000	3	26	3	18.61	-67.70	33	4.5	Md	4.0
216	2000	3	30	9	18.82	-68.01	46	4.3	Md	3.8
217	2000	4	4	23	18.97	-67.31	4	3.3	Md	3.1
218	2000	4	7	2	18.27	-67.58	6	3.3	Md	3.0
219	2000	4	8	7	18.16	-67.36	18	3.4	Md	3.2
220	2000	4	10	11	18.95	-64.23	84	4.0	Md	3.6
221	2000	4	10	22	18.67	-66.80	25	3.8	Md	3.0
222	2000	4	13	18	19.64	-63.29	33	4.2	mb	3.9
223	2000	4	18	2	19.08	-69.52	89	4.5	mb	3.9
224	2000	4	30	3	18.46	-67.97	22	3.6	Md	3.4
225	2000	5	3	1	17.67	-62.86	200	3.6	Md	3.6
226	2000	5	4	2	17.80	-65.62	3	3.3	Md	3.1
227	2000	5	8	5	19.45	-68.50	33	4.5	mb	3.9
228	2000	5	15	5	18.24	-66.35	35	3.5	Md	2.9
229	2000	5	20	22	19.38	-67.26	56	3.8	Md	3.5
230	2000	5	26	9	19.04	-63.88	10	3.8	Md	3.6
231	2000	6	1	21	19.42	-65.42	49	4.6	Md	4.3
232	2000	6	11	20	19.91	-70.85	33	4.4	Md	4.3
233	2000	6	18	10	17.93	-66.84	16	3.1	Md	3.1
234	2000	6	23	8	19.41	-65.19	76	3.6	Md	3.6
235	2000	6	24	2	18.08	-65.73	3	3.2	Md	3.0
236	2000	6	25	10	19.39	-65.11	66	3.8	Md	3.3
237	2000	7	5	12	18.40	-65.89	34	3.5	Md	3.0
238	2000	7	7	14	18.93	-66.76	53	3.3	Md	3.0
239	2000	7	24	15	18.15	-67.01	21	3.3	Md	3.0
240	2000	7	26	2	17.85	-61.51	33	4.0	mb	3.9
241	2000	7	28	9	18.70	-64.29	71	4.1	Md	3.6
242	2000	7	28	15	18.93	-64.68	62	4.4	mb	4.2
243	2000	7	29	7	17.84	-68.70	33	4.4	mb	4.3
244	2000	7	30	18	18.79	-69.42	87	3.9	Md	3.7
245	2000	7	31	11	18.77	-64.65	25	4.0	Md	3.3
246	2000	8	1	23	17.46	-68.24	117	4.2	Md	3.7
247	2000	8	2	1	18.39	-66.65	13	3.6	Md	2.9

248	2000	8	12	9	18.03	-66.60	15	3.6	Md	2.9
249	2000	8	15	9	19.16	-66.84	57	3.3	Md	3.2
250	2000	8	16	8	18.40	-65.91	105	3.2	Md	3.1
251	2000	8	17	6	18.11	-64.74	60	3.3	Md	3.2
252	2000	8	19	0	18.06	-65.51	0	3.6	Md	3.0
253	2000	8	19	8	17.92	-66.94	3	3.8	Md	3.3
254	2000	8	31	1	18.75	-64.00	74	4.1	Md	3.5
255	2000	9	3	12	18.70	-66.73	12	3.5	Md	2.7
256	2000	9	4	6	19.27	-65.99	107	3.5	Md	3.2
257	2000	9	4	15	19.05	-66.32	43	3.6	Md	3.4
258	2000	9	5	20	19.00	-68.09	113	4.1	Md	3.4
259	2000	9	7	0	18.87	-65.26	35	3.4	Md	3.1
260	2000	9	12	16	17.97	-65.93	5	3.6	Md	2.8
261	2000	9	15	6	18.87	-67.47	32	3.4	Md	3.3
262	2000	9	18	10	20.06	-70.07	33	4.4	mb	4.3
263	2000	9	22	23	19.02	-64.93	25	4.0	Ml	3.4
264	2000	9	23	22	19.26	-64.15	21	4.0	Md	3.3
265	2000	9	24	7	19.47	-66.07	64	3.7	Md	3.2
266	2000	9	25	5	19.23	-62.56	33	4.7	Md	4.2
267	2000	9	25	6	19.19	-62.52	33	4.9	mb	4.0
268	2000	9	25	23	18.12	-67.29	18	3.3	Md	3.0
269	2000	9	27	7	19.11	-64.79	50	3.7	Md	3.2
270	2000	9	28	6	19.26	-66.68	48	3.8	Md	3.2
271	2000	9	29	19	19.36	-66.27	27	3.7	Md	3.1
272	2000	9	30	2	19.42	-65.12	28	3.9	Md	3.5
273	2000	10	1	19	18.88	-64.66	25	3.5	Md	3.2
274	2000	10	2	15	18.90	-68.31	41	4.0	Md	3.7
275	2000	10	2	17	18.17	-67.41	7	3.7	Md	3.4
276	2000	10	8	11	18.78	-64.26	37	3.7	Md	3.2
277	2000	10	9	5	19.19	-65.40	90	3.9	Md	3.5
278	2000	10	11	1	18.93	-64.41	25	3.7	Md	3.2
279	2000	10	11	4	18.98	-66.60	68	3.1	Md	3.0
280	2000	10	13	0	18.64	-66.47	71	3.3	Md	3.1
281	2000	10	14	2	19.04	-67.42	30	3.2	Md	3.1
282	2000	10	15	0	18.55	-65.11	20	3.6	Md	3.0
283	2000	10	16	12	19.21	-64.48	45	4.0	Md	3.5
284	2000	10	16	13	19.25	-65.85	33	3.7	Md	3.0
285	2000	10	17	3	18.81	-67.34	6	3.5	Md	3.1
286	2000	10	17	8	19.65	-68.68	13	4.0	Md	3.6
287	2000	10	22	3	19.03	-64.96	68	3.8	Md	3.2
288	2000	10	23	5	18.79	-65.03	53	3.8	Md	3.2
289	2000	10	25	16	17.85	-66.91	41	3.8	Md	3.1
290	2000	10	25	21	17.86	-66.91	39	3.9	Md	3.4
291	2000	10	27	18	17.65	-61.17	42	4.7	Md	4.5
292	2000	10	27	19	17.60	-61.19	37	5.6	Md	5.2
293	2000	10	29	3	17.98	-66.94	16	3.6	Md	3.2
294	2000	10	30	14	18.71	-67.34	21	3.7	Md	3.4
295	2000	11	1	10	18.44	-67.05	102	3.4	Md	3.2
296	2000	11	6	3	18.00	-68.81	94	3.6	Md	3.5
297	2000	11	16	19	19.84	-65.13	24	4.0	Md	3.9
298	2000	11	25	11	17.78	-65.97	46	3.2	Md	2.8

299	2000	11	30	16	18.63	-66.71	85	4.1	Md	3.8
300	2000	12	1	11	18.56	-66.68	86	3.1	Md	3.0
301	2000	12	1	15	19.30	-67.95	55	4.3	Md	4.1
302	2000	12	8	8	17.86	-68.55	35	3.7	Md	3.5

mb Body wave Magnitude
Md Duration Magnitude
Ml Local Magnitude
Mw Moment Magnitude

Table 2. Ground Motion Relations for Puerto Rico (Horizontal Component, generic soft rock site, NEHRP C)

$log\ PSA\ (f, R) = c_1 + c_2(\mathbf{M}-6) + c_3\ (\mathbf{M}-6)^2 + hingeFunction + c_4 R$

$R = (D^2 + \Delta^2)^{0.5}$

$\Delta = -7.333 + 2.333\ \mathbf{M}$

hingeFunction = (-1.8 + 0.1 **M**) log (*R*) for R ≤ 75 km

hingeFunction = (-1.8 + 0.1 **M**) log (*75*) for 75 km ≤R ≤ 100 km

hingeFunction = (-1.8 + 0.1 **M**) log (*75*) - 0.5 log (*R*/100) for R ≥ 100 km

PSA is 5% damped horizontal component pseudo-acceleration in cm/sec^2; *f* in hertz; **M**, Moment magnitude; D = closest distance to fault surface in km. All logs are in Base 10. Standard deviation 0.28 in log10 units is suggested for all frequencies.

f (Hz)	c_1	c_2	c_3	c_4
0.10	1.62	0.91212	-0.10486	-0.00092
0.13	1.80	0.90635	-0.11886	-0.00081
0.16	1.98	0.89009	-0.13157	-0.00064
0.20	2.16	0.87177	-0.14444	-0.00052
0.25	2.36	0.84583	-0.15306	-0.00048
0.32	2.55	0.81112	-0.16625	-0.00044
0.40	2.74	0.78035	-0.17792	-0.0005
0.50	2.89	0.73416	-0.1706	-0.00056
0.63	3.04	0.67664	-0.15973	-0.00061
0.79	3.20	0.63441	-0.15706	-0.0008
1.00	3.35	0.56986	-0.14377	-0.00086
1.26	3.47	0.497	-0.11945	-0.00105
1.59	3.58	0.47303	-0.11486	-0.00118
2.00	3.68	0.44246	-0.10831	-0.00126
2.51	3.74	0.40472	-0.08864	-0.00139
3.16	3.83	0.38087	-0.09045	-0.00159
3.98	3.88	0.35932	-0.07932	-0.00185
5.01	3.94	0.33077	-0.06816	-0.00204
6.31	3.97	0.33046	-0.07344	-0.00219
7.94	3.98	0.32515	-0.07216	-0.00234
10.00	3.96	0.32088	-0.06542	-0.00244
12.59	3.94	0.32165	-0.06523	-0.00253
15.85	3.88	0.33249	-0.06818	-0.00251
PGA	3.60	0.35181	-0.06926	-0.00201
PGV	2.35	0.54828	-0.06350	-0.00107

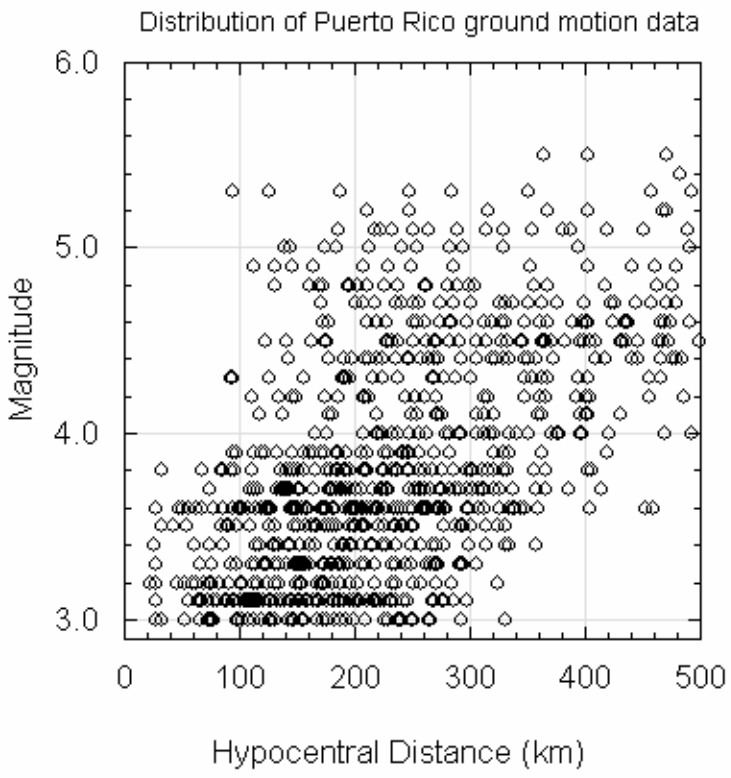

Figure 1. Distribution of study events in magnitude and distance.

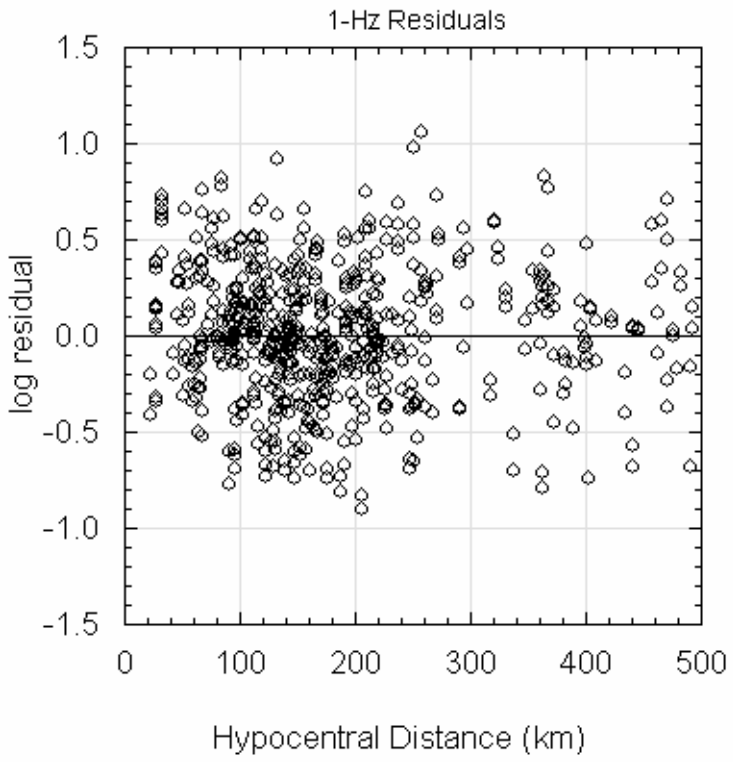

Figure 2. Distribution of residuals versus distance for hinge points 75, 100km and f = 1.0 Hz.

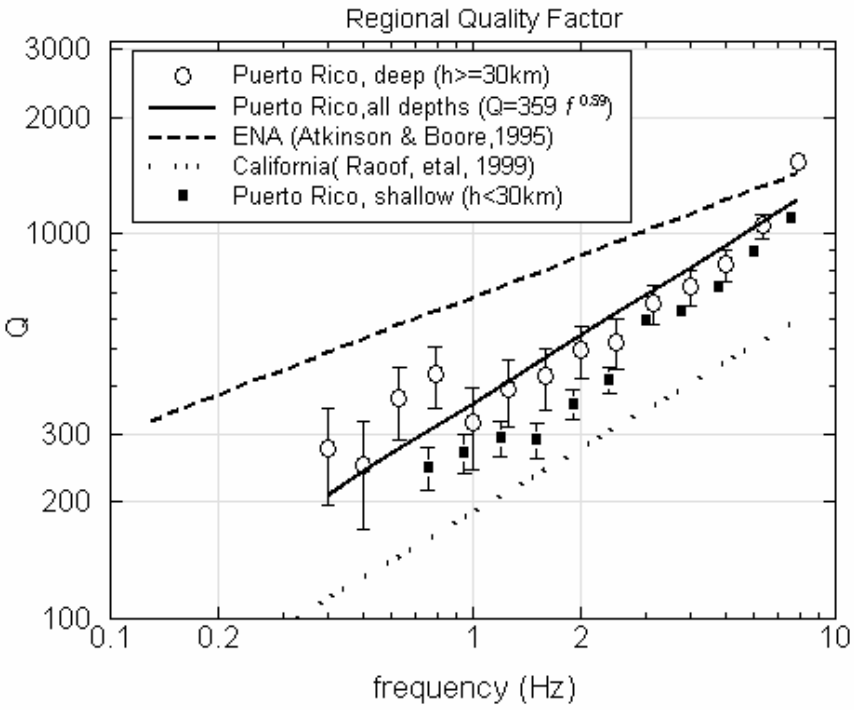

Figure 3. Q value for Puerto Rico compared to Eastern North America (Atkinson and Boore, 1995) and California (Raoof et al, 1999). Error bars show standard error of Q. Differences between Q for deep and shallow events in Puerto Rico are not significant.

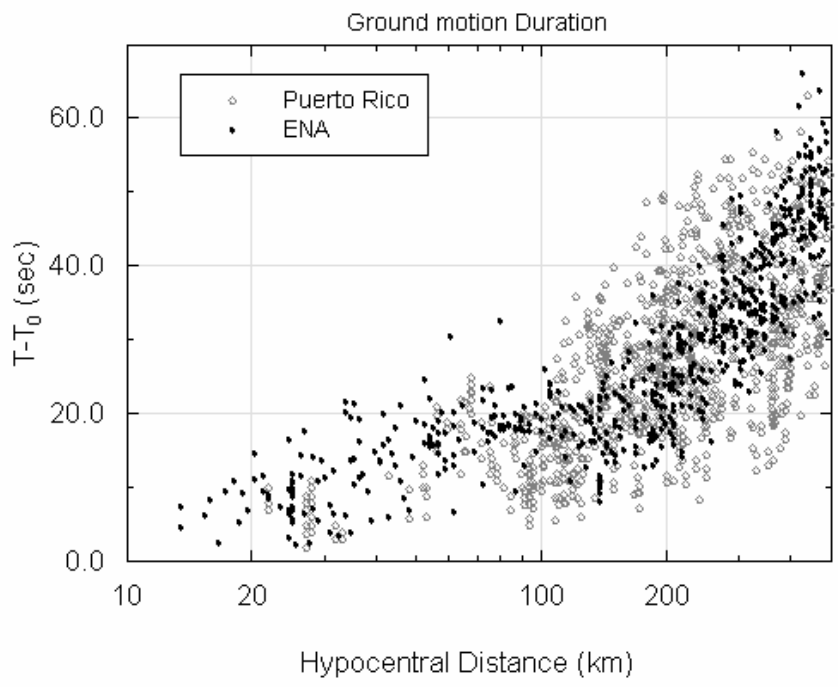

Figure 4. Comparison between duration distribution of ENA and Puerto Rico (ENA data are from Atkinson and Boore 1995). Duration measure is total duration – source duration, where source duration is small (<1 sec) for these events. The change of slope at around 75 and 100km suggests a trilinear attenuation curve for the Puerto Rico region, similar to observations for Eastern North America.

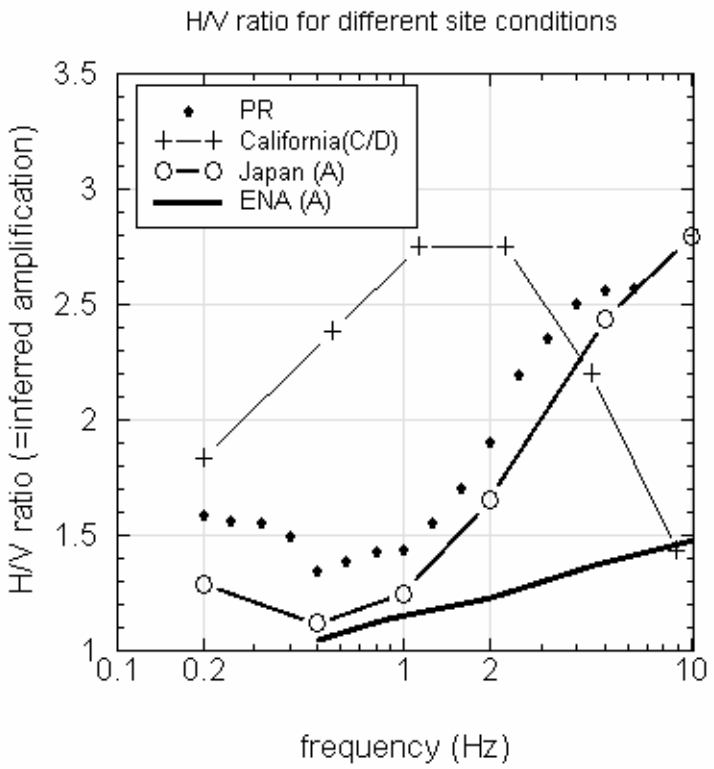

Figure 5. H/V ratio for Puerto Rico (site SJG) in comparison to that for other regions. Letters give NEHRP site class.

Figure 6. Profile of observation points around earthquake fault.

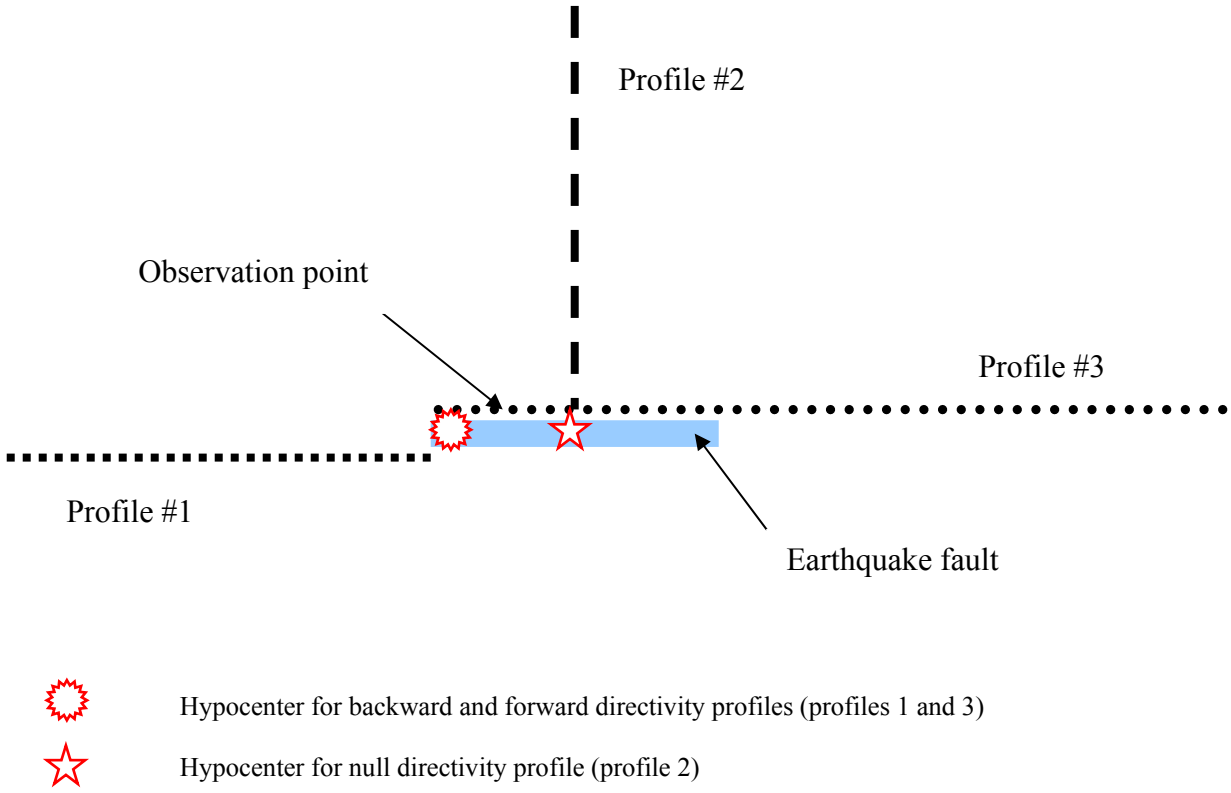

Figure 6. Profile of observation points around the earthquake fault used in simulations.

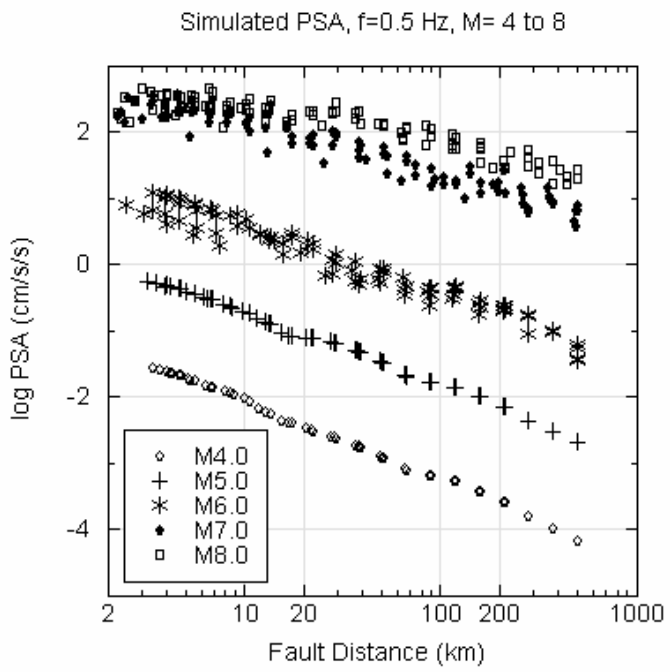

Figure 7. Horizontal-component response spectra (PSA) of Simulated Acceleration Time Series at 0.5 Hz versus distance for different magnitudes. Each of three directivity cases is plotted.

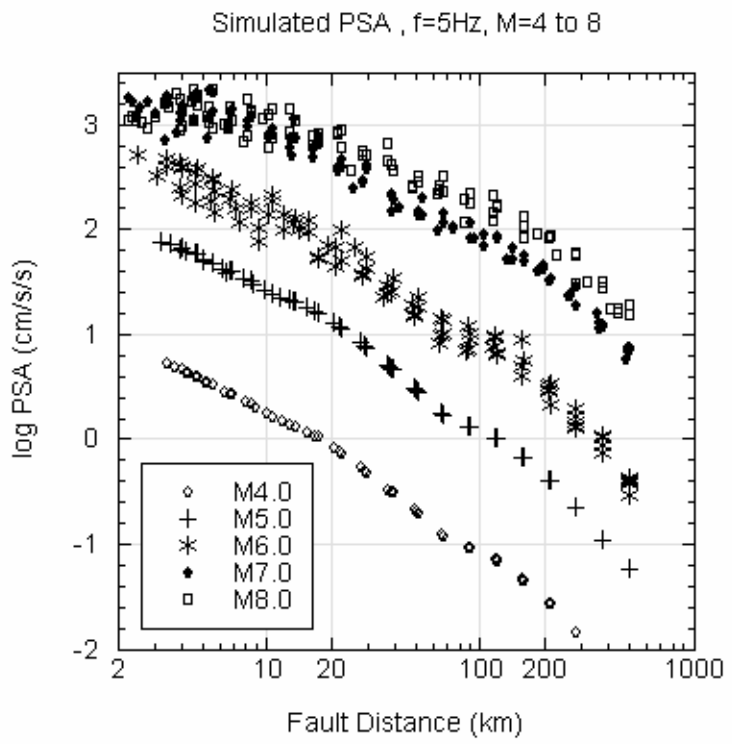

Figure 8. Horizontal-component response spectra (PSA) of Simulated Acceleration Time Series at 5 Hz versus distance for different magnitudes; each of 3 directivity cases is plotted.

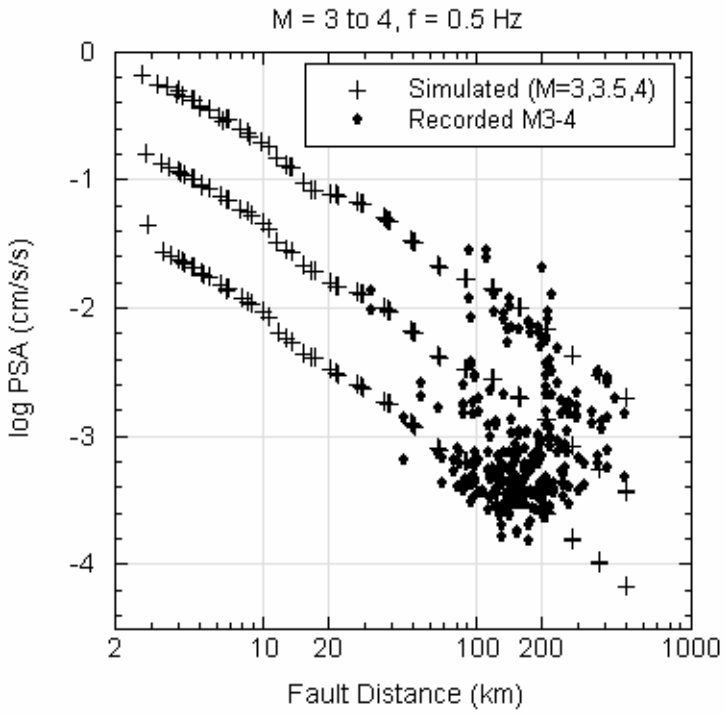

Figure 9. Simulated PSA at M 3.0, 3.5, 4.0, in comparison to PSA from the recorded data, M3.0-M4.0, f=0.5Hz.

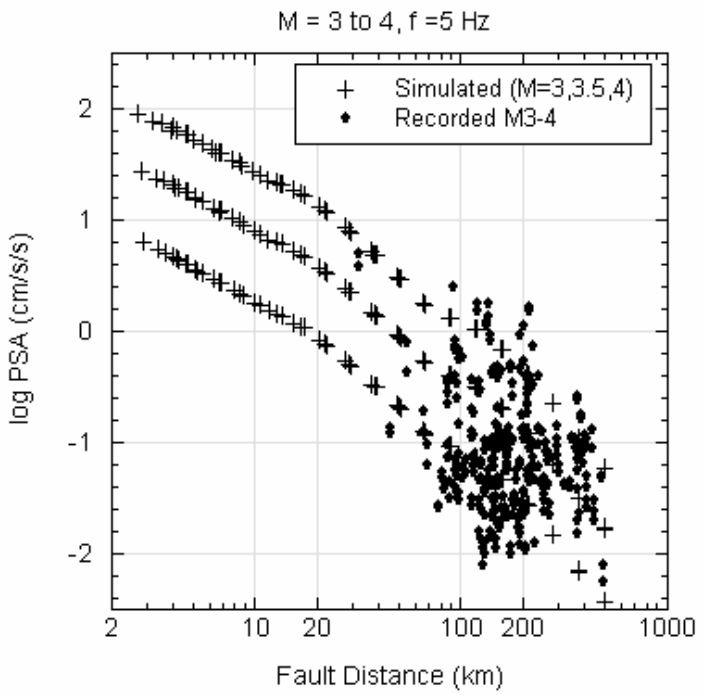

Figure 10. Simulated PSA at M 3.0, 3.5, 4.0, in comparison to PSA from the recorded data, M3.0-M4.0, f=5Hz.

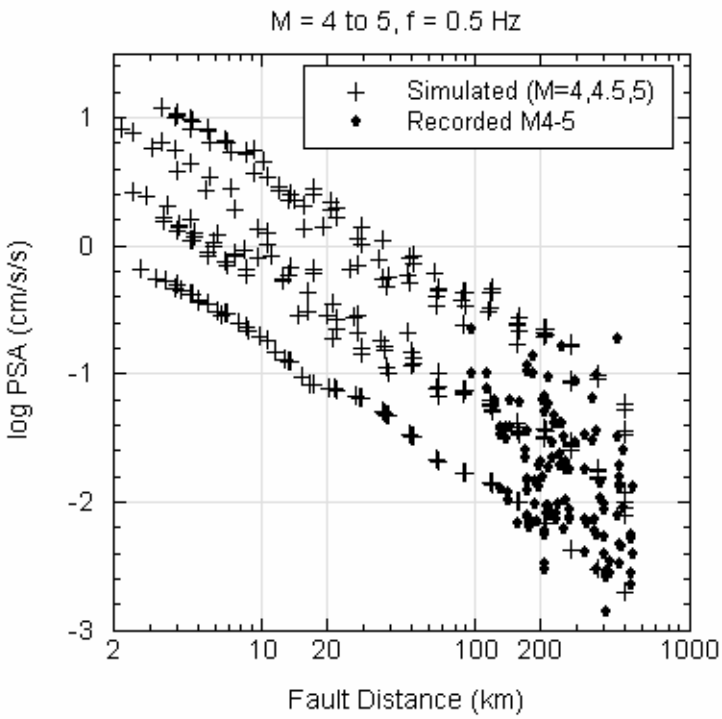

Figure 11. Simulated PSA at M 4.0, 4.5, 5.0, in comparison to PSA from the recorded data, M4.0-M5.0, f=0.5Hz.

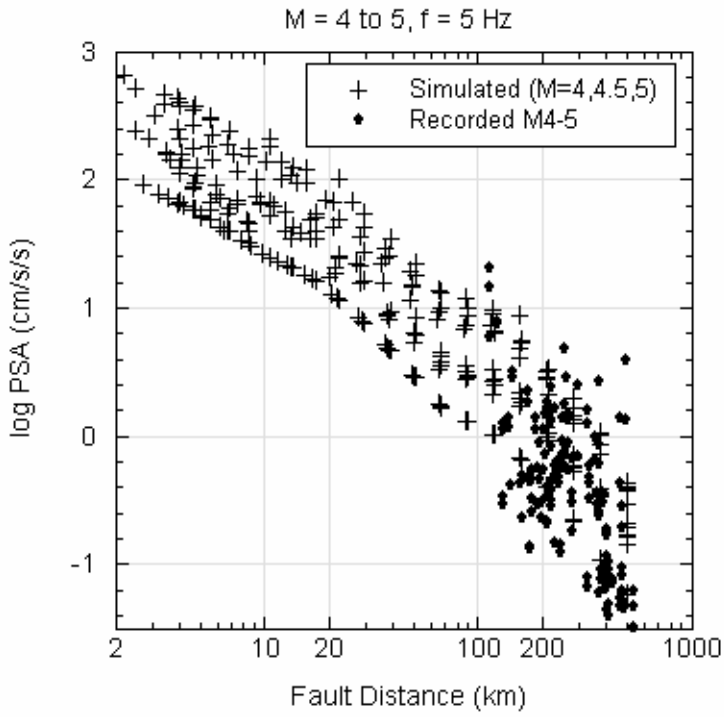

Figure 12. Simulated PSA at M 4.0, 4.5, 5.0, in comparison to PSA from the recorded data, M4.0-M5.0, f=5.0Hz.

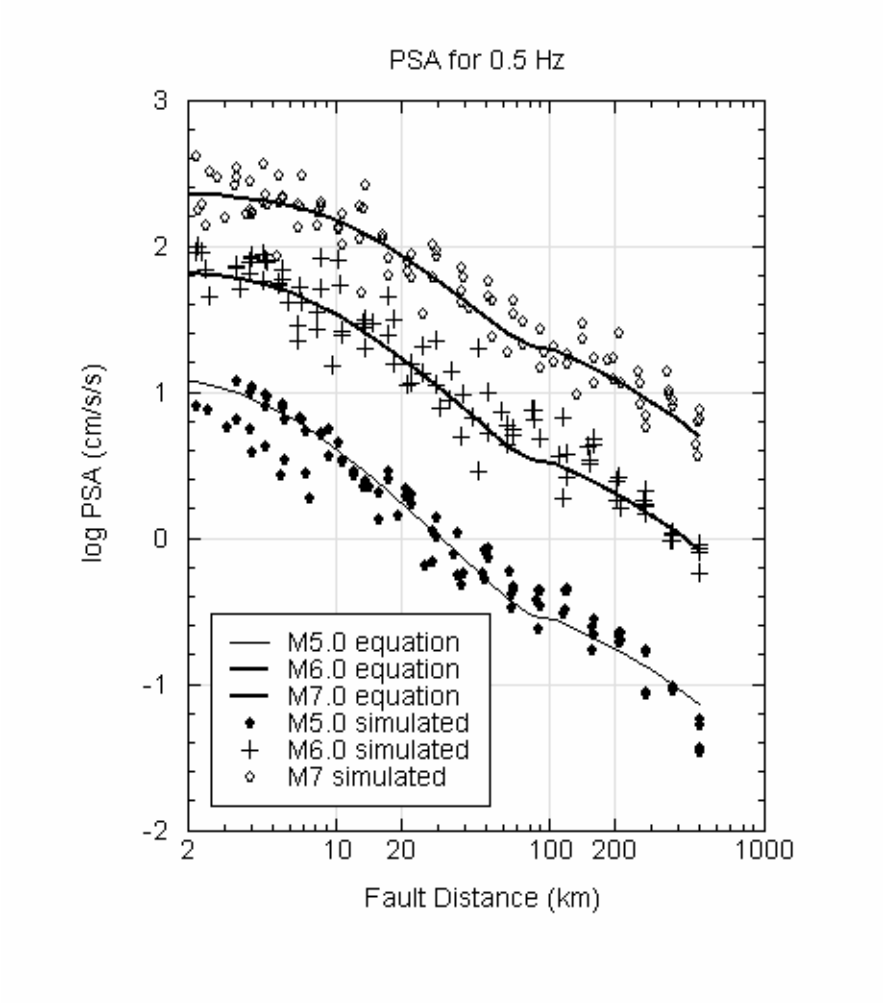

Figure 13. Comparison between the developed ground motion equations and the simulated data, f=0.5Hz.

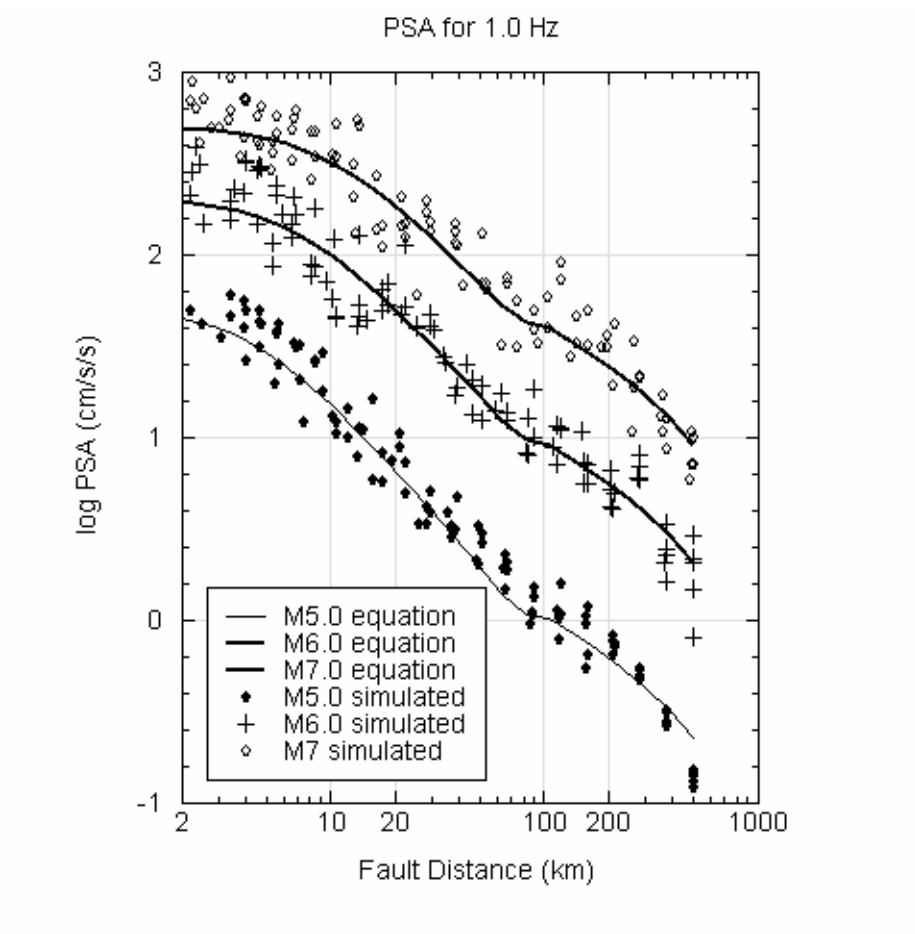

Figure 14. Comparison between the developed ground motion equations and the simulated data, f=1.0Hz.

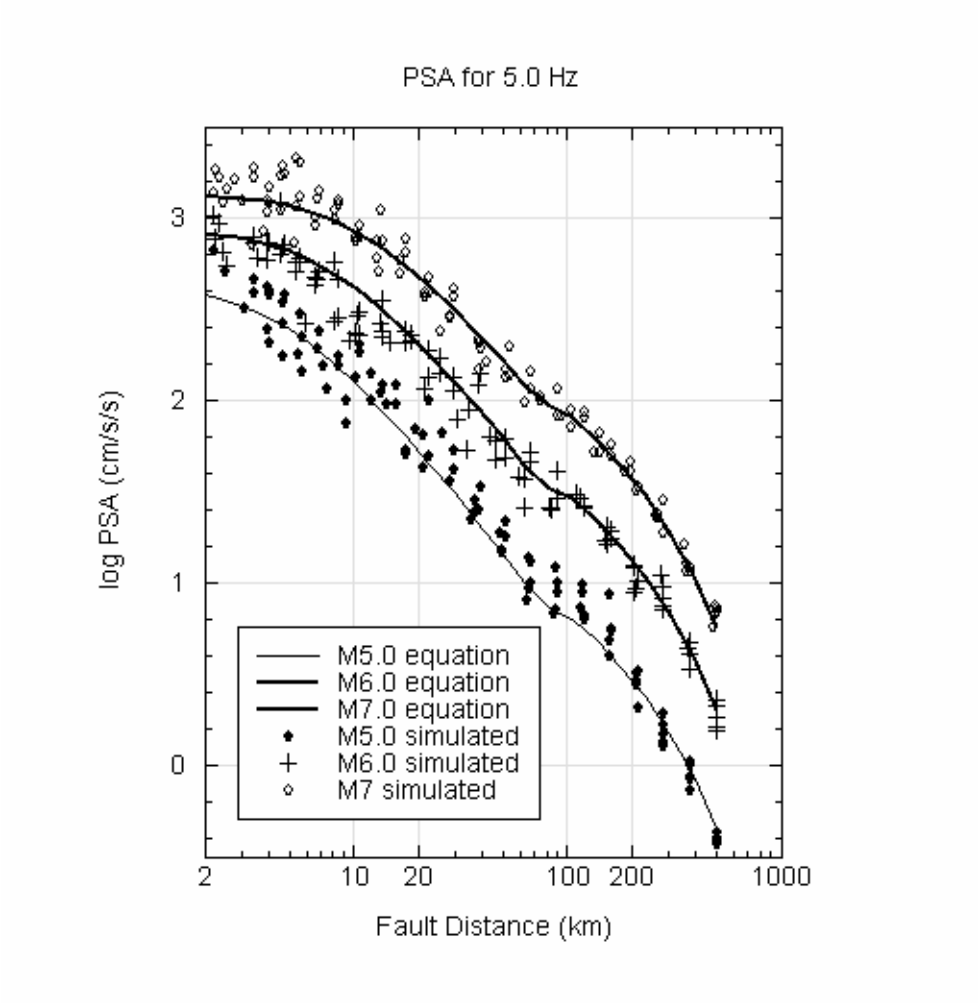

Figure 15. Comparison between the developed ground motion equations and the simulated data, f=5.0Hz.

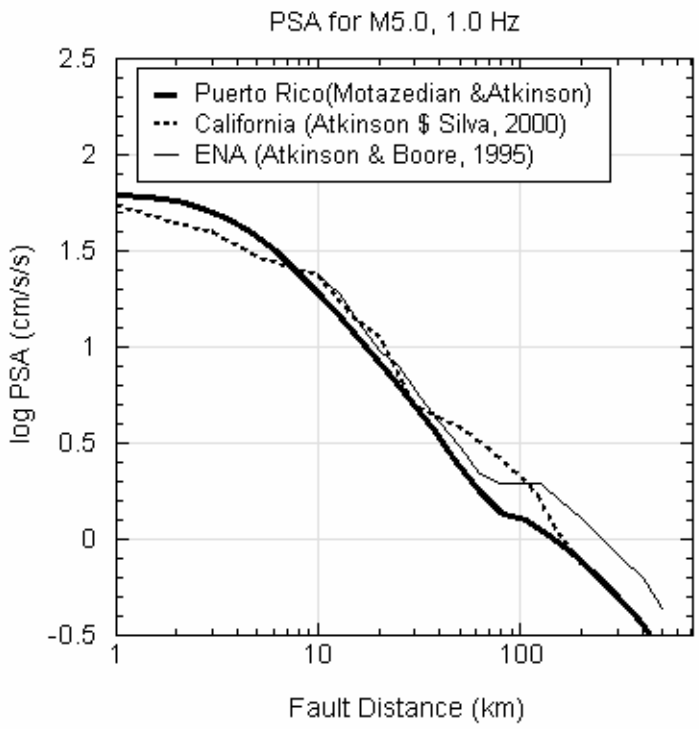

Figure 16. Ground motion relations for Puerto Rico compared to other regions. PSA for M5.0, f=1.0 Hz. All relations plotted for NEHRP C site conditions.

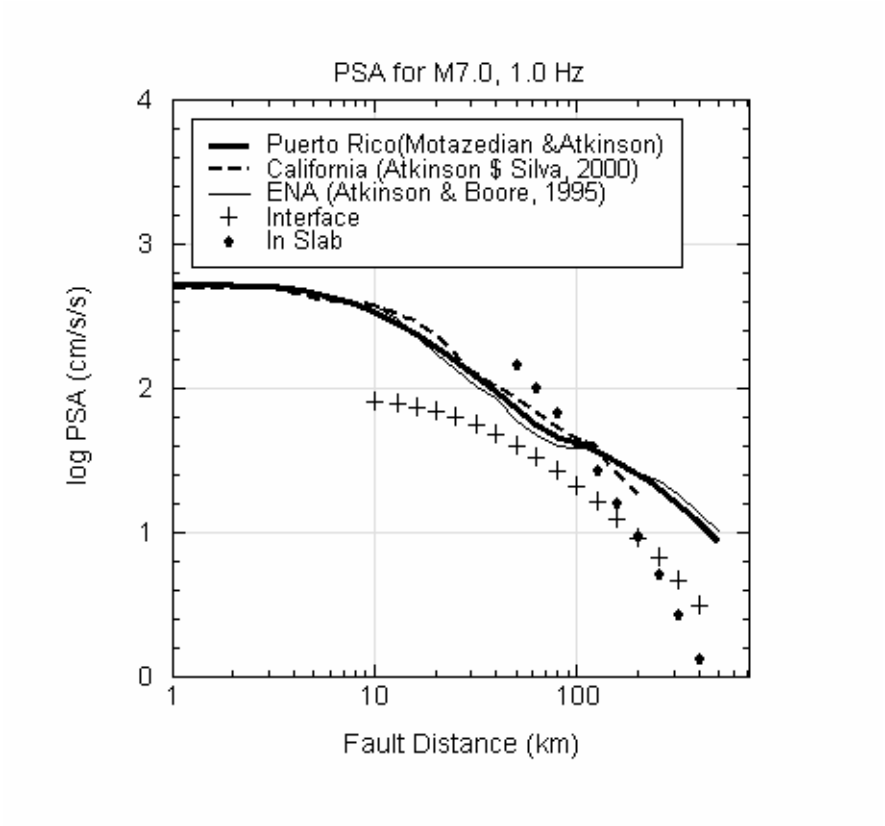

Figure 17. Ground motion relations for Puerto Rico compared to other regions. PSA for M7.0, f=1.0 Hz. All relations plotted for NEHRP C site conditions.

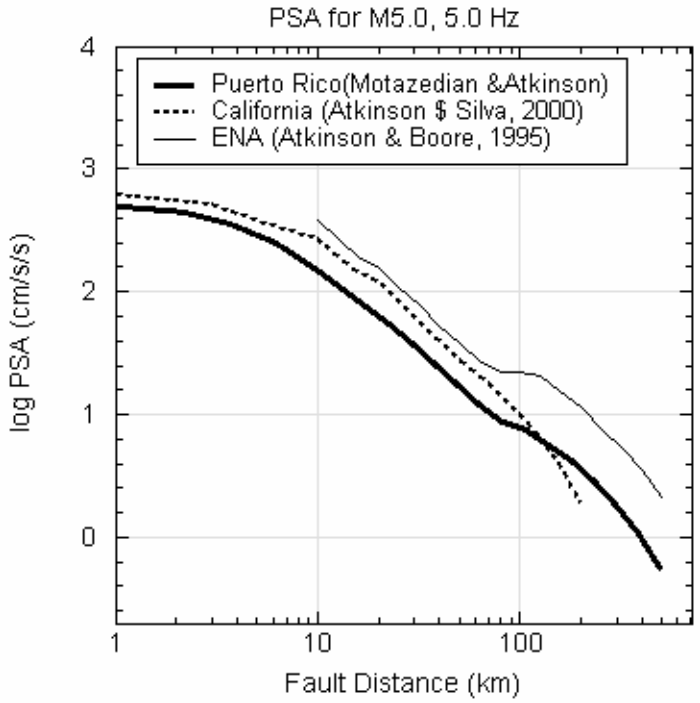

Figure 18. Ground motion relations for Puerto Rico compared to other regions. PSA for M5.0, f=5.0 Hz. All relations plotted for NEHRP C site conditions.

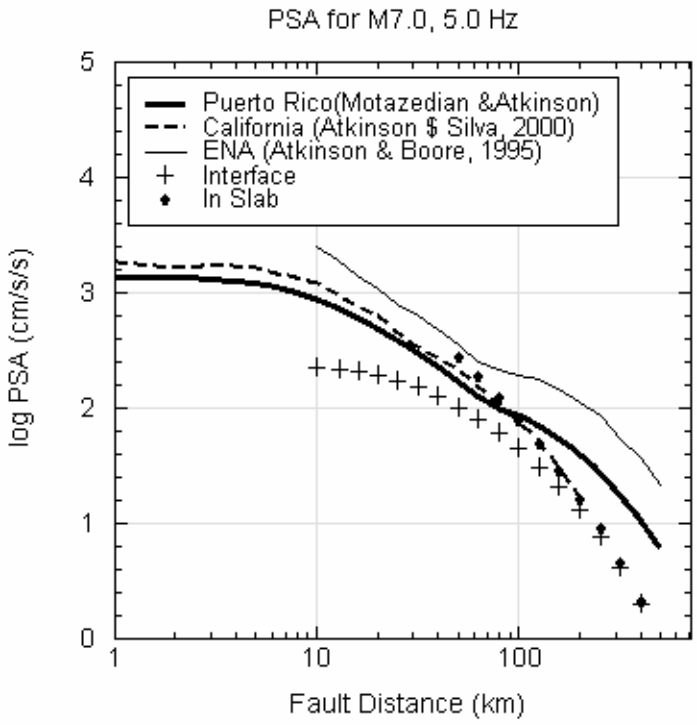

Figure 19. Ground motion relations for Puerto Rico compared to other regions. PSA for M7.0, f=5.0 Hz. All relations plotted for NEHRP C site conditions.